https://doi.org/10.5194/egusphere-2025-2088
Preprint. Discussion started: 26 May 2025

Post-glacial reshaping of Alpine topography induced by landsliding

Coline Ariagno[1,2], Philippe Steer[1], Pierre G. Valla[2], Benjamin Campforts[3]

[1]Université Rennes, Géosciences
[2]ISTerre, Grenoble CNRS
[3] Department of Earth Sciences, VU University Amsterdam, Netherlands

Correspondence to : Coline Ariagno (coline.ariagno@unive-rennes.fr)

Abstract. In steep alpine environments, successive glacial-interglacial cycles during the Quaternary led to multiple transient geomorphological phases. In particular, post-glacial periods are key transition phases experiencing rapid geomorphic changes, characterized by intense hillslope processes where ice and permafrost have retreated. Mass wasting is the dominant post-glacial process driving sediment production in steep mountain landscapes. However, its role in shaping topography, particularly in comparison to glacial activity—known for its strong deformational impact—remains poorly understood. By integrating numerical modeling with topographic data, we refine our understanding of how mass wasting shapes evolving landscape and influences sediment dynamics. In the Ecrins massif (French western Alps), we select three catchments, with particular morphological signatures or inheritance (i.e. from fluvial to glacial) to model their associated topographic evolution driven by mass wasting. Using the landscape evolution model 'HyLands', we quantitatively assess their individual response to landsliding by exploring the role of different internal or external factors (e.g., bedrock cohesion, return time of landslides). The model is calibrated with the output landslide area-volume scaling law and the massif-averaged denudation rate, inferred from literature. We focus on the cumulative impact of landslides, over a single post-glacial period, on catchment slope distribution, hypsometry, produced sediment volume and erosion rate. Compared to ~~fluvial ones~~, inherited glacial topography shows a bimodal distribution of elevation for unstable slopes, near the crests and along the U-~~shape~~ valley walls. The time evolution of this distribution is characterized by a decrease in the number of unstable slopes as well as a lowering in maximum catchment elevations induced by landsliding, usually attributed to the glacial buzzsaw. Indeed, glaciers may be not the only agent controlling mountain elevation, as we ~~discussed in this study.~~ Despite the stochastic nature of landslides, our modeling results also show that landslide activity and induced erosion rates are ~~maximum~~ at the onset of the glacial retreat and then ~~progressive~~ decay during the interglacial period. ~~On the contrary,~~ fluvial catchments show a more stable topography and less intense landslide activity resulting in lower erosion rates. This study quantitatively explores the non-linear interactions between landslides and catchment topographic evolution and questions the role of landslides in the erosion pulse during ~~the~~ Quaternary interglacial periods.

https://doi.org/10.5194/egusphere-2025-2088
Preprint. Discussion started: 26 May 2025

1. Introduction

The Quaternary period is characterized by oscillations from glacial to interglacial cycles overprinting a global climatic cooling trend over the Cenozoic era (Zachos et al., 2001). These successive climatic transitions have been suggested to be associated with abrupt and transient geomorphologic and topographic changes (Champagnac et al., 2014; Peizhen et al., 2001). In high-latitude regions and mountain ranges, glaciers are usually considered as the main geomorphic and erosion agents (Hallet et al., 1996; Herman et al., 2013, 2021; Herman & Champagnac, 2016; Métivier et al., 1999). The topographic changes resulting from glacial erosion are progressive and spatially variable over a single or multiple glacial-interglacial cycle (Seguinot & Delaney, 2021) of the Quaternary (Herman et al., 2011; Pedersen & Egholm, 2013; Sternai et al., 2013; Tomkin & Braun, 2002). Glaciated landscapes have in turn been widely studied to better understand past glacier dynamics and quantify glacial erosion rates and associated topographic changes at the Earth's surface (Ganti et al., 2016; M. Koppes et al., 2015; Pedersen & Egholm, 2013; Peizhen et al., 2001; Solomina et al., 2015; Sternai et al., 2013). Glacial and periglacial processes have strongly imprinted mountainous landforms, shaping U-shaped valleys, but also cirques, arêtes and hanging valleys, all characterized by steep slopes and rugged topography (e.g. Anderson et al., 2006; Penck, 1905; Prasicek et al., 2015). In turn, glacial morphological features likely represent transient and mechanically unstable landforms under interglacial conditions (Herman & Braun, 2008; Prasicek et al., 2015), dominated by hillslope and fluvial processes. Understanding the interglacial evolution of formerly glaciated landscapes has remained challenging since it involves complex non-linear geomorphic processes and interrelated spatial/temporal scales. Yet, this is a major need for assessing the ongoing response of mountainous environments to current climate warming (e.g. Zhang et al., 2022).

Interglacial periods are associated with overall warming climatic conditions, leading to a progressive cryosphere degradation (i.e. glacier retreat and permafrost recession), and in turn to a shift of the main geomorphic and erosion processes. Under interglacial conditions, paraglacial (Ballantyne, 2002) and periglacial (French, 2017) processes become more efficient and affect larger mountainous areas. Hillslope processes, including landsliding, rockfall and soil creep, affect formerly glaciated mountain slopes. Rivers transport remobilized and newly-produced sediments (Roussel et al., 2018) and can locally re-incise glacial valleys (e.g. Leith et al., 2018; Valla et al., 2010). Over the Quaternary, repetitive climatic oscillations between glacial and interglacial periods have caused frequent mismatches between dominant geomorphological processes and the organization or shape of the landscape on which they act. This has led to the hypothesis that these transient climatic/geomorphic conditions over the Quaternary could have led to an increase in erosion, sediment flux (M. Koppes et al., 2015; M. N. Koppes & Montgomery, 2009; Peizhen et al., 2001) and topographic relief (Champagnac et al., 2014), rather than the supposed greater efficiency of glacial erosion itself (Koppes and Montgomery, 2009).

https://doi.org/10.5194/egusphere-2025-2088
Preprint. Discussion started: 26 May 2025

In the following work, we focus on the transient phase from glacial to interglacial conditions, hereinafter referred to as the post-glacial period, i.e. when alpine glaciers retreated and left uncovered landscape dominated by non-glacial geomorphic agents. In this context, steep parts of mountain hillslopes become more prone to mass wasting processes, favored by glacial debuttressing (E. Cossart et al., 2008) and permafrost retreat (e.g. Cathala et al., 2024; Lebrouc et al., 2013). The rapid climate change observed over the last decades has motivated research on the evolution of permafrost and its impact on high-elevation rockwall dynamics (Gallach et al., 2020; Magnin et al., 2017; Ravanel et al., 2017; Stoffel et al., 2024). In addition, gravitational instabilities, such as bedrock landslides or rockfalls, are widespread in mountainous landscapes and appear as one of the most efficient processes to shape them (Keefer, 1984). Taking over glacial erosion, hillslope activity transiently reshapes glacial morphological features leading to a postglacial increase in both the frequency and intensity of hillslope events through time (e.g. Korup, 2006; Zerathe et al., 2014). Landslides significantly contribute to catchment-scale erosion by mobilizing large bedrock volumes, which greatly impact sediment fluxes (Broeckx et al., 2020; Hovius et al., 1997; Zech et al., 2009). As a positive feedback loop, by decreasing the local baselevel, fluvial sediment export and incision of formerly glaciated valleys, can foster the hillslope response. The postglacial period is also associated to major changes in the hillslope-channel connectivity (Brardinoni & Hassan, 2007; Cavalli et al., 2019; Müller et al., 2022) and in the drainage system (Comiti et al., 2019; Lane et al., 2017; Pitlick et al., 2021; Zhang et al., 2022). As such, this period appears complex due to rapid morphological changes and multiple geomorphic processes that all interact and drive major changes in both the hillslope domain and the drainage network. Therefore, quantifying the spatio-temporal impact of landslides on evolving postglacial landscapes is needed to better understand sediment production, transfer and potential storage along the source to sink pathway and assess the overall topographic evolution in mountainous environments.

If the landsliding impact on mountain topography appears clear after a single triggering event, such as a storm or an earthquake (Dahlquist et al., 2018; Meunier et al., 2008; Morriss et al., 2023; J. Roering, 2012), their role in long-term shaping of mountain range is not straightforward. For investigating the post-glacial period, landslide catalogues (Blondeau et al., 2021; Wood et al., 2015), bedload records (Lane et al., 2017), remote-sensing and geophysical methods have intrinsic limitations and integration times that are too short. Conversely, long-term mountain erosion estimates from geochronological and thermochronological methods (Herman et al., 2013) or large-scale sediment budgets (Kuhlemann et al., 2002) may have too long integration times to investigate interglacial periods. Terrestrial cosmogenic nuclides (TCN) have been commonly used to quantify catchment-wide erosion rates over 10^2 – 10^5 yr timescales (Brown et al., 1995; Delunel et al., 2020; Mudd et al., 2016; Portenga & Bierman, 2011), covering glacial-interglacial cycles. Although this approach appears meaningful to address the postglacial period (~10-20 kyr), TCN-derived erosion rates are punctual and averaged in both space (catchment) and time. In turn, this prevents exploring in detail the spatial distribution and temporal

https://doi.org/10.5194/egusphere-2025-2088
Preprint. Discussion started: 26 May 2025

evolution of erosion during that period. Moreover, the cosmic ray attenuation depth, which sets the integration time of TCN (von Blanckenburg, 2005), can be significantly smaller than the depth of large ~~to gigantic~~ landslides observed in formerly glaciated catchments (Korup, 2006; Lavé et al., 2023). Overall, this raises the question of the potential limitations of TCN-derived erosion rates in constraining the time evolution of post-glacial erosion in landscapes dominated by bedrock landsliding.

In this context, landscape evolution modelling (LEM) appears as a relevant approach to overcome the limited amount of data/observations and the intertwined spatial and temporal scales involved (Tucker & Hancock, 2010). Numerical modelling can combine complex surface processes, including tectonic uplift, hillslope and river dynamics integrating all the sediment transfer cascade and hillslope-channel connectivity, while allowing predictions over large spatial and temporal scales. Different categories of models can be considered to study mass wasting processes (Campforts et al., 2022). ~~Physical~~-based models produce realistic debris-flow (and river) propagation and deposition but may not be adapted for large-scale landscape evolution (Croissant et al., 2017; Davy et al., 2017; Dietrich et al., 1995; George & Iverson, 2014; Hergarten & Robl, 2015; Martin et al., 2023). Landscape evolution models (LEM) ~~rather~~ use reduced-complexity geomorphic laws to simulate the evolution topography over possibly long timescales and large spatial scales (Carriere et al., 2020; Langston & Tucker, 2018; Liebl et al., 2021). For instance, linear or non-linear diffusion laws are generally used to simulate hillslope erosion in most LEMs (Heimsath et al., 2005; Perron, 2011; ~~J. J.~~ Roering et al., 1999). Soil-covered models simulate shallow landslides to follow for instance the impact of rainfall variability at large scale (Claessens et al., 2007), while bedrock-landslide models allow the distinction between constant and episodic sediment production through landslides (Campforts et al., 2020; Densmore et al., 1998). Therefore, numerical modelling offers multiple ways to simulate ~~hillslopes~~ processes, and their interactions, by highlighting diverse approaches, modeling complexity and spatio-temporal scales.

The aim of this study is to explore numerically, using a reduced-complexity model, the role of landslides in the postglacial morphological dynamics of mountainous landscapes. We use the HyLands model (Campforts et al., 2020, 2022), which explicitly ~~simulate~~ bedrock landslides, to predict associated mass redistribution and the resulting catchment-averaged erosion rates and topographic evolution through multiple timescales. We investigated the topographic impact of landslide activity on selected Alpine catchments, located in the Ecrins massif (France), showcasing a gradient of glacial imprint and deglaciation timing. An open question is the role of interglacial processes in erasing the inherited morphological signature of former glaciation, leading to an erosional ‘‘hot-moment”. More specifically, we aim to assess the timescales, rates and locations of topographic changes associated with the transient shift from glacial to interglacial periods, with a particular focus on the role of landsliding. Our working hypothesis is that the different morphological signatures observed for Alpine catchments are evidencing both landslide activity and deglaciation timing. The first objective of the study is to conduct a spatial analysis of simulated landslides to assess their magnitudes and locations within investigated catchments.

https://doi.org/10.5194/egusphere-2025-2088
Preprint. Discussion started: 26 May 2025

Then, a temporal analysis is performed to investigate whether the postglacial period remains a transient phase and how long it may require to achieve an interglacial steady-state topography and erosion dynamics under landslide activity.

2. Study area

2.1 ~~Tree selected~~ catchments in the Ecrins massif

The Ecrins massif (south-east France, Fig. 1A) forms a high-elevation high-relief area of the southwestern Alps, and today still hosts glaciers in its upper catchments. The present-day topography was deeply impacted by glaciation (van der Beek & Bourbon, 2008), and several studies have focused on constraining the timing and extent of the Last Glacial Maximum (LGM, ca. 20 ka) and post-LGM glacier fluctuations (Delunel et al., 2010; Le Roy et al., 2017). In this context, we select three small (6 – 15 km^2 area) catchments to cover the entire Vénéon valley, from the river source, at the heart of the Ecrins massif, to the confluence with the Romanche river where tributary glaciers had a lower morphological impact (Fig. 1B). The Pilatte catchment, the highest and most glaciated catchment, peaks at ~3600 m above sea level (a.s.l.), ~~with valley bottoms around~~ 2000 m. Modern glaciers represent ~14% of the ~~catchment area~~ (total catchment area of approximately 15 km²). With a downstream direction toward the north, its western and eastern parts are made of granitic ~~or~~ migmatic rocks (gneiss), respectively (source: French Geological Survey BRGM). The Etages catchment, partially-glaciated at present~~-day~~ (~12 %), displays similar characteristics with an area of ~14 km² and an elevation range from 3564 to 1600 m a.s.l. at the confluence with the Vénéon river. The catchment is mainly underlaid by granites with crestlines composed of gneiss in its south-eastern part (Barféty et al., 1984; Delunel et al., 2014). Both catchments show steep hillslopes (>45-60°, Fig. 1C), located on the walls of the main U-shaped valley and along the highest rockwalls, considered as nunataks (Delunel et al., 2010; Marx et al., 2017), and a low-relief central valley bottom (Fig. 1D). The Etages catchment has been investigated by Delunel et al., 2014, with ~~a~~ detailed geomorphological mapping and use of ~~quartz~~ ^{10}Be concentrations in detrital material to trace the potential geomorphic sources for river sediments. ~~The third catchment, called "La Pisse",~~ is completely unglaciated today and is smaller than the two other catchments (~6 km² total area). Its highest elevation at ~3050 m occurs at its southern crest, while its lowest elevation ~1250 m is at the confluence with the adjacent Villard catchment. Its lithology is dominated by granites ~~even if the southwestern crest shows few Jurassic limestone outcrops.~~ Slopes are mostly gentle in the upper part of the catchment and get steeper downstream along the valley rockwalls. Despite different glacial imprints and elevation, the slope ~~distribution~~ for the studied catchments ~~is~~ relatively similar (Fig. 1C), with a modal slope around 35° (0.7 m/m) for all three catchments.

These 3 investigated catchments have experienced a gradual post-LGM deglaciation, following the progressive glacier retreat along the Vénéon valley from downstream (Pisse catchment) to upstream

https://doi.org/10.5194/egusphere-2025-2088
Preprint. Discussion started: 26 May 2025

(Pilatte catchment). Following Delunel (2010), the Pisse catchment has likely started its deglaciation around 15 ka, while the Etage catchment may have been deglaciated between 13 and 7 ka. The glacier retreat in the Pilatte catchment has probably started slightly after the Etage catchment and can be considered at the end of the post-LGM deglaciation. As a consequence, the observed delay in glacier retreat between the three catchments (Fig. 1A) has likely been associated with a time-transgressive activation of periglacial processes like landslides, resulting in different topographic configurations today.

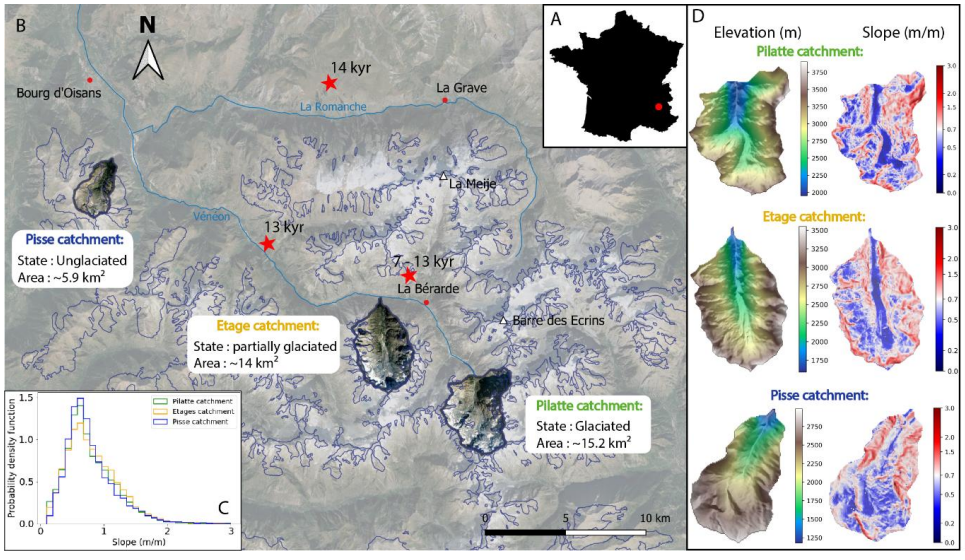

Figure 1: Geomorphological context of the study area. A) Location of the Ecrins massif (red dot) in France. B) Google satellite image of the Ecrins massif (background) with the three studied catchments and their characteristics: Pilatte (green label), Etages (yellow label) and Pisse (blue label). Blue thin line indicates the contour of the LGM ice extent (Delunel, 2010). Red stars report the estimated deglaciation timing (Delunel, 2010). C) Probability density function of topographic slope for the three studied catchments (25-m resolution DEM from the French National Geographic Institute IGN). Similar distributions are observed, with a main slope mode around 0.7 m/m. D) Modern elevation and slope maps for the three studied catchments.

2.2 Characteristics of glacial-catchment profiles

To visualize the hillslope morphologies in our studied catchments, we made topographic transects (Fig.2) along the main valley. In the literature or on the field, classical glacial topographic features, including typical U-shape valleys (Fig. 3), are well documented, easily observable and have been suggested to result from the bimodal distribution of glacial erosion with elevation (e.g. Anderson et al., 2006; Egholm et al., 2009; Herman et al., 2011; Steer et al., 2012). The observed bimodal hypsometry of glacial landscapes (Brocklehurst & Whipple, 2006) defines the boundaries between the valley overdeepening, driven by fast-moving ice with intense abrasion and quarrying, and areas with slower-moving ice exerting less erosive power (Coutterand, 2010; Leith et al., 2014). Alternatively, this bimodal hypsometry may be attributed to different patterns of cold-climate erosion around the ELA (Liebl et al.,

https://doi.org/10.5194/egusphere-2025-2088
Preprint. Discussion started: 26 May 2025

2021). In both interpretations, the hillslope shoulder – a slope inflection between ~~two steep~~ hillslopes, ~~known as "shouldering"~~ - is shaped during glacial periods (Louis, 1952; Valla, 2021). This topographic shouldering would result in a bimodal distribution of catchment elevations with steep slopes associated to both the glacier valley flanks (low elevations) and to the nunataks-crestlines area (i.e. periglacial regions at high elevations) (Coutterand, 2010; Liebl et al., 2021).

~~In our studied catchments, the~~ two upper catchments (Pilatte and Etages catchments) ~~highlight the~~ U-shaped valley on each transect, even in the upstream part of the catchment. A slope ~~inflexion~~ is also visible along most of the ~~transect~~, which we ~~refer to as "shouldering"~~ (Fig. 3). For most of the transects, the increase in slope furthest upstream corresponds to the glacial trimline (Penck, 1905). It corresponds to the highest zone of the glacier extent and usually the limit between prevailing glacier erosion processes and periglacial processes, as their elevations match with the upper limits of the glacier cirque (Rootes & Clark, 2020) (Fig. 2). Conversely, the topographic transects for the unglaciated catchment (Pisse) tend to reveal a V+-shape valley, especially in the lower part of the catchment. The upper profile, however, is closer to those of the glacial and intermediate ~~catchment~~, showing a clear inheritance from previous glaciations.

In the following, we will name the three studied catchments according to their glacial morphology imprint, i.e 'glacial', 'intermediate glacial-fluvial' and 'fluvial' for the Pilatte, Etages and Pisse catchments, respectively.

https://doi.org/10.5194/egusphere-2025-2088
Preprint. Discussion started: 26 May 2025

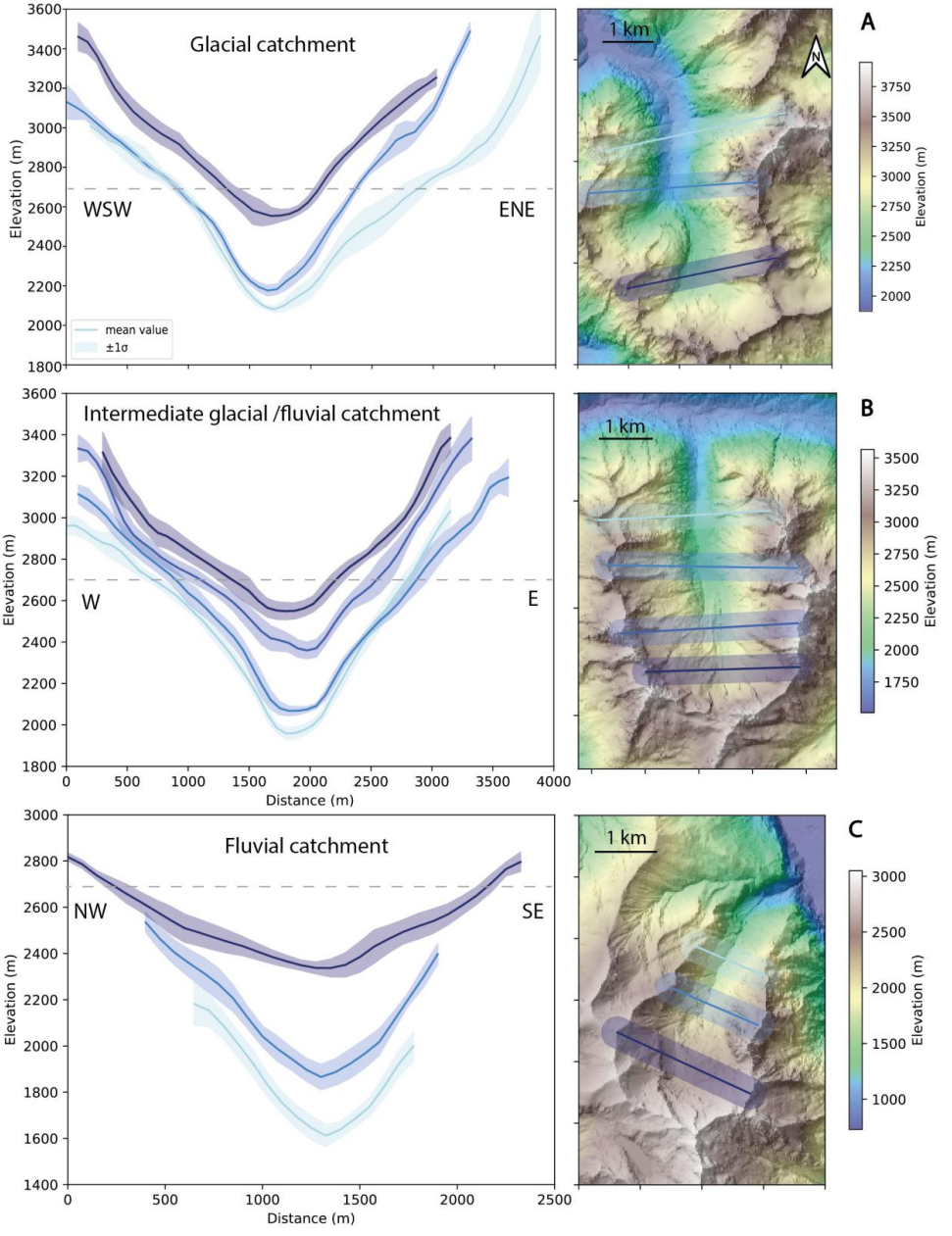

Figure 2: Swath topographic profiles for the three different catchments (Lehmann & Robert, 2024) (DEM, resolution: 50 cm, ESPG2154, from the French National Geographic Institute, Cusicanqui, 2024): (A) Glaciated catchment (Pilatte), (B) intermediate glacial-fluvial catchment (Etages), and (C) fluvial catchment (Pisse). Profiles are aligned based on their lowest area. The grey dot line illustrates the 2700 m elevation, a threshold elevation where the predicted landslides activity is lower (Figs. 6 & 7).

https://doi.org/10.5194/egusphere-2025-2088
Preprint. Discussion started: 26 May 2025

3. Modeling framework

Hylands is a reduced-complexity and stochastic landslide model (Campforts et al., 2020, 2022). It simulates both the erosion associated with deep-seated gravitational landslides and the induced sediment transport and deposition resulting from landslide runout. Hylands is part of the Landlab open-source framework (Barnhart et al., 2020; Hobley et al., 2017), which offers tools to combine multiple geomorphic laws on 2D regular grids, potentially applied to either synthetic topographies or digital elevation models (DEMs). In the following, we use the 25-m resolution DEMs from the BD ALTI of IGN (French National Geographic Institut), as initial model topographies for the three studied catchments. The catchment boundaries were obtained from the geo-processing tools ("Eau France" service website: https://reseau.eaufrance.fr/geotraitements/viewer/bassin-versant). We first here present the model and then our strategy for model calibration.

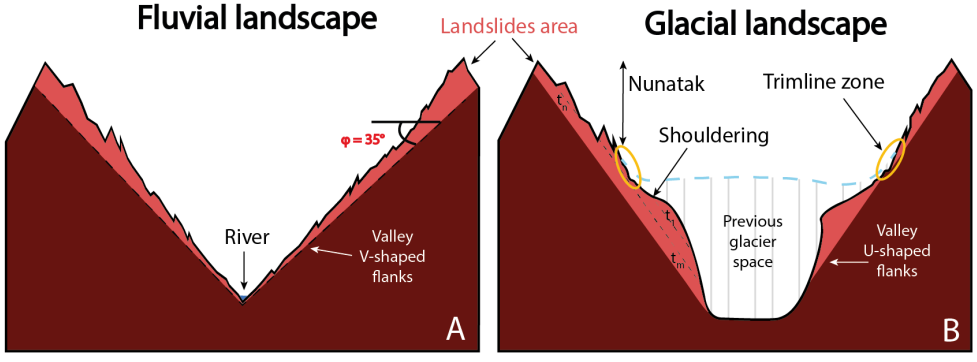

Figure 3: Conceptual sketches of theoretical ~~topographic~~ fluvial (A) and glacial (C) landscapes. A) Typical landscape dominated by fluvial erosion processes with V-shaped valley and homogeneous hillslopes slightly above the internal angle of friction (φ = 35° in this example). B) Landscape dominated by glacial erosion processes. The main morphological characteristics such as U-shaped valley, periglacial nunatak zone, shouldering ~~or~~ the trimline zone (yellow circle) are shown (modified from Louis, 1952; Coutterand, 2010). The light-red color indicates potential landscape areas affected by landslide activity.

3.1 The HyLands model

3.1.1 Landslide triggering

In HyLands, the landslide source model combines a spatial probability P_s and a temporal probability P_t to compute a landslide failure probability $P_{failure} = P_s * P_t$. The spatial probability is computed following a modified Culmann criterion (Campforts et al., 2020; Culmann, 1875), which is a Mohr-Coulomb criterion applied to a finite slope analysis:

$$P_s = \frac{H_s}{H_c}, \qquad with \quad H_c = \frac{4C}{\rho g} \frac{\sin\beta \cos\varphi}{1-\cos(\beta-\varphi)}, \tag{1}$$

where H_s (m) is the local hillslope height calculated between two adjacent cells of the grid and H_c is the maximum stable hillslope height (m), which depends on the cohesion C (kg.m^{-1}.s^{-2}), ρ the rock density

https://doi.org/10.5194/egusphere-2025-2088
Preprint. Discussion started: 26 May 2025

set to 2700 kg.m^{-3}, g = 9.81 m.s^{-2} the gravitational acceleration, β the local topographic angle, and φ the angle of internal friction (Eq. 1). Both C and φ are parameters that need to be calibrated in our modelling approach.

However, HyLands is not a deterministic model as it combines this spatial probability of failure to a temporal probability. Indeed, P_t controls the temporal occurrence of landslides and follows a Poisson law (Campforts et al., 2022):

$$P_t = 1 - e^{-t/t_{LS}}, \quad (2)$$

where t (yr) is the model time and t_{LS} (yr) is the return time of landslides triggering events. In turn, the probability of failure of a given cell increases with time, until $P_{failure}$ becomes greater or equal to one, leading to landslide triggering. The simulation time step is set to dt = 10 yr.

3.1.2 Landslide erosion and deposition

When a landslide event is triggered, the erosion scar generates a failure plan which initiates at the triggering point. Following the Culmann criterion, the dip angle of this plan θ, is the bisector of the local topography angle β, and the angle of internal friction of the material φ:

$$\theta = \frac{\beta + \varphi}{2} \quad (3)$$

The failure plane is propagated upstream of the critical node if the elevation of the neighboring cells exceeds the rupture surface. In this case, all the DEM cells above this surface are considered as unstable and mobilized by landsliding.

Landslide-derived sediments can either be transported as wash load, determined by the fraction of fines, Ff in the model, or redistributed using a non-local nonlinear deposition scheme (Campforts et al., 2022). Because our first goal is to study landslide erosion without any potential feedback of deposited sediments, we set the fraction of fine sediments Ff to 1, meaning that all sediments are instantaneously evacuated. It also means that in our set-up no topographic change can occur below the triggering points of simulated landslide sources.

3.2 Strategy for model calibration

Our objective is to use a calibrated and physically sound landscape evolution model, based on HyLands, to predict landslide activity during postglacial conditions in our study area. Note that in these simulations, we only consider the role of landslides in landscape evolution and erosion dynamics, without modeling fluvial erosion nor tectonic activity (e.g., uplift rate). We also assume that gravitationally triggered landslides as simulated in HyLands, represent the combination of mass wasting events in alpine topography including rockfalls, debris flows, and shallow to deep-seated landslides, capturing the diverse range of slope failure processes. Our model calibration is performed on the Etages catchment following two steps:

https://doi.org/10.5194/egusphere-2025-2088
Preprint. Discussion started: 26 May 2025

1) Calibrating φ and C, which control the spatial probability of landslide occurrence, by comparing the modelled landslides area-frequency distribution (3.3.2) and size-volume scaling relationship (3.3.3), with the ones of natural landslide datasets (Fig. 4; Delgado et al., 2022; Guzzetti et al., 2002).
2) Calibrating the landslide return time t_{LS}, which sets the temporal probability of landslide occurrence, by comparing modelled catchment-averaged erosion rates and observed erosion data derived from quartz ^{10}Be concentrations in stream sediments (3.3.4, Fig. 5), ranging between 0.27 and 1.1 mm/yr in the Ecrins massif (Delunel et al., 2010). For the Vénéon valley and the studied catchments (i.e. Etages catchment), we can reduce the interval from 0.7 to 1.1 mm/yr for our model calibration (Fig. 5). Assuming that a rock sample records quartz ^{10}Be accumulation over the time period corresponding to the upper 60 cm below the surface (Delunel et al., 2010; von Blanckenburg, 2005), ^{10}Be-derived erosion rates record apparent integration times of around 500 to 2500 yr. We thus select a simulation time of 1500 yr for the model calibration phase.

Some combinations of parameters (φ, C, t_{LS}) lead to too few landslides, preventing a statistical analysis of their resulting size distribution. To overcome this issue, we generated a large amount of landslide events and selected a similar number of landslides per simulation. Then, we had to(1) compile multiple simulations with similar parameters but different stochastic occurrence (different seeds), (2) reduce the return time (t_{LS} = 100). Because t_{LS} controls the occurrence of landslides without impacting their geometry, a small value of t_{LS} induces simulation outputs with large landslide datasets. This is particularly true given that the potential for landsliding remain significant throughout the simulation. The first approach was used for all the parameter calibration (Figs. 4A-C, 5), while the second approach was only used in the landslide size-frequency calibration (Fig. 4A) because the modified return time value can induce changes in landslide volumes and occurrences, and thus in output catchment-averaged erosion rates (Fig. 5).

3.3 Model calibration

3.3.1 Calibration of the angle of internal friction: landslide area-frequency distribution

Because we are lacking detailed compilation of alpine mass-wasting events, HyLAnds will be calibrated against global compilations of landslide data. More specifically, we aim at constraining the cohesion and angle of internal friction parameters. Although not calibrated to our specific field site, this general calibration will allow assessing the impact of gravity driven erosion in high alpine terrain and therefore provides sufficient for this study. For our calibration runs, we run HyLands from existing topography of the three catchments and set model parameters not involved in the calibration equal to those as reported in Table S1.

https://doi.org/10.5194/egusphere-2025-2088
Preprint. Discussion started: 26 May 2025

Field inventories of landslides and rockfalls show a well-known shape for the frequency distribution of landslide area, highlighting several characteristics of a power-law relationship (Delgado et al., 2022; Guzzetti et al., 2002; Jeandet et al., 2019; Malamud et al., 2004; Stark & Hovius, 2001; Tanyaş et al., 2019; Tebbens, 2020): (1) the rollover value, matching the highest frequency of the landslide-area distribution, (2) the power-law scaling exponent, α, defined from the slope of the linear regression measured for large landslides events and (3) the cutoff value, related to the divergence of the distribution from a power-law scaling. With the exception of few parameter combinations (in the range of tested parameters of friction and cohesion), the simulated landslides size-frequency distributions we obtained not display any clear rollover. This lack of rollover is probably due to the coarse resolution of the grid (25 m) which makes it impossible to visualize small landslides. we do not use this criterion for our model calibration approach. The power-law scaling exponent is a key parameter as it describes the frequency of intermediate to large landslides, which convey most of the eroded volume. This exponent also varies significatively with the internal angle of friction (Fig. 4B). As no power-law exponent value exists for the French Alps landslide-rockfall inventories, we use as a reference the mean value α_{mean} = -2.3 suggested by (Van Den Eeckhaut et al., 2007) from a global landslide compilation. (Tanyaş et al., 2018, 2019) also carried out a landslide compilation and analysis of landslide size-frequency distributions, proposing a slightly higher power-law exponent (α_{mean} = -2.5). However, this inventory only considers earthquake-induced landslides. In addition, power-law exponents tend to be smaller for igneous or metamorphic rock (such as present in our study area) (Bennett et al., 2012), so we retain the value of -2.3 for our model calibration. In our calibration phase, we set the cutoff area at 3. 10^4 m² based on the shape of the linear regression fit and the good value of the Pearson correlation coefficient (Fig. 4A). Our cutoff value seems to be smaller but overall consistent with previously reported values (Tanyas et al., 2018; 2019).

The simulated landslide size-frequency distribution (Fig. 4A), in a log-log plot, illustrates the decrease in landslide number when increasing landslide size. From all simulated landslides (5. 10^4 in total; see Section 3.2), we randomly select 20 000 landslides to construct the landslide size-frequency distribution. This method ensures a homogeneous number of events between different combinations of input parameters (Fig. 4B). Therefore, we compare the simulated power-law scaling exponent α, resulting from different combinations of cohesion (C) and internal friction angle (φ), with the literature power-law exponent of -2.3. The power-law regression is computed using a log-log linear fit. The output matrix (Fig. 4B) shows a gradient for the power-law exponent α with increasing φ values. In our simulations, α varies strongly, between -1.7 and -3.1, when changing the internal angle of friction (31-39°, Fig. 4B). This range is consistent with global compilations of power-law exponents for landslide-area scaling (Tanyaş et al., 2018, 2019; Van Den Eeckhaut et al., 2007). We also observe little variability in α with cohesion (C). Therefore, we fix the internal angle of friction at $\varphi = 35°$ which leads to simulated values of α close to -2.3. As the cohesion parameter seems to not influence the power-law exponent of the

https://doi.org/10.5194/egusphere-2025-2088
Preprint. Discussion started: 26 May 2025

landslides size-frequency distribution, we calibrate this parameter using an alternative strategy (see section 3.3.3).

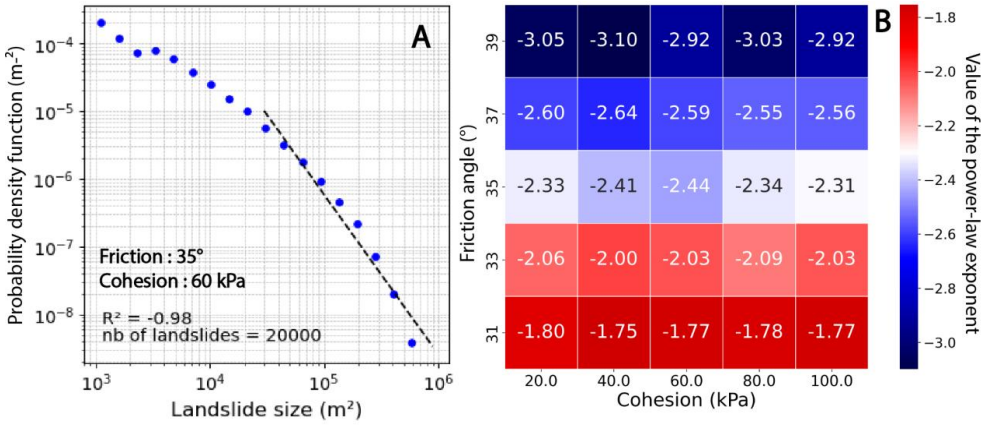

Figure 4: Calibration approach for the internal angle of friction and the cohesion in ~~HyLand~~ model. Calibration outcomes result from multiple simulations, with similar input parameters, to get a larger dataset of landslides (see text for discussion). A) Landslide size distribution, with a linear fit (dashed black line) on the power-law tail of the distribution. The cutoff value (i.e minimum size where the linear fit starts) is set to 3. 10^4 m². B) Calibration matrix between the internal angle of friction (φ) and the cohesion (C). The angle of friction is calibrated based on the minimum difference between the power-law exponent of the simulated size distribution and the reference value (-2.3; van den Eeckhaut et al., 2007). Blue colors indicate output power-law exponents smaller than the reference value (-2.3, white colors) and red colors indicate predicted power-law exponents higher than the reference value.

As a verification of our model calibration, we also simulate the area-volume relationship for simulated landslide distributions (Fig. S1). The relevant cloud of landslides events (n=426) shows a power-law scaling similar to those observed elsewhere with an intercept value of 0.84 and an exponent value γ=1.49 (Fig. S1) (Larsen et al, 2010; Wood et al, 2015).

3.3.3 Calibration of landslide return time and cohesion: ^{10}Be-derived erosion rate

To calibrate the cohesion and the landslide return time parameters, we compare simulated and ^{10}Be-derived catchment-averaged erosion rates (3.2, Fig. 5). Both model parameters impact nonlinearly the output erosion rate, and increasing t_{LS} or C leads to lower output erosion rates (Fig. 5). Several combinations of parameters predict an output catchment-averaged erosion rated within the expected range (0.7 – 1.1 mm/yr): 1) a high C=100 kPa associated with a short t_{LS}=80 kyr, 2) a small C=40 kPa associated with a long t_{LS}=250 kyr, or 3) an intermediate parameter combination with C=60 kPa and t_{LS}=150 kyr. These three model parameterizations also lead to roughly similar spatial and temporal patterns in landslide activity. In the following, we therefore use the intermediate parameter combination (Fig. 5).

https://doi.org/10.5194/egusphere-2025-2088
Preprint. Discussion started: 26 May 2025

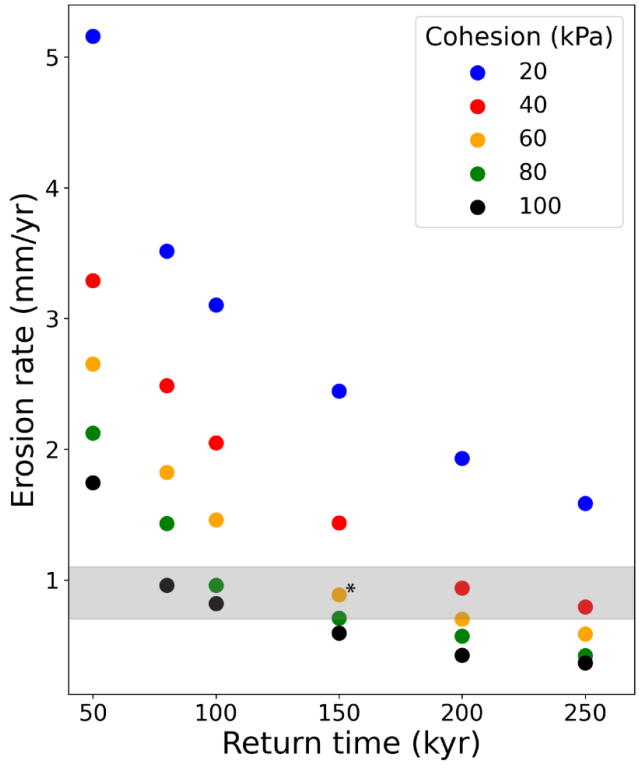

Figure 5: Calibration of the landslide return time and cohesion parameters based on the simulated catchment-averaged landslide erosion rate. Considering the calibrated angle of internal friction (35°, Fig. 4B), each dot represents a particular combination of landslide return time and cohesion (color code indicating the cohesion value). The selected combination is identified with a ~~stars~~ (*). The simulated erosion rate is an averaged catchment-scale erosion rate over a compilation of 20 different simulations (1500 yr duration). The grey band illustrates the range of ~~literature values~~ (0.7-1.1 mm/yr; Delunel et al., 2010).

4. Results

4.1 Spatial and temporal distribution of landslide activity

Using the calibrated model, we investigate the impact of landslide activity on catchment topographic changes over ~~100 kyr (timescales for glacial-interglacial cycles)~~. Over this timescale, the calibrated landscape evolution model generates different spatial patterns of landslide erosion across the three studied catchments (Fig. 6). In each catchment, landslide erosion is distributed heterogeneously, ranging from areas experiencing ~~an~~ intense landslide activity and significant topographic changes to overall unaffected areas. For the ~~Pilatte catchment (glacial),~~ significant topographic changes, up to 500 m, occur along its northeast ridges. Elsewhere, predicted landslides lead to smaller topographic ~~changes,~~ around 100 m (Fig. 6A). The intermediate glacial-fluvial ~~catchment (Etages),~~ shows erosion patches along its crests and summit walls. In some areas, ~~cumulated~~ erosion reaches 350 m, while shallower landslides are observed on low-elevation hillslopes, just above the valley bottom (Fig. 6B). For the ~~Pisse catchment (fluvial),~~ landslide erosion is mainly focused on the downstream parts of the catchment where the valley narrows and slopes become steeper. ~~Cumulated~~ landslide erosion reaches up to 250 m, ~~however, the~~

https://doi.org/10.5194/egusphere-2025-2088
Preprint. Discussion started: 26 May 2025

upper part of the catchment shows limited landslide activity (Fig. 6C). The final slopes across the three catchments clearly highlight the locus of landslide activity. Indeed, landsliding results in homogeneous slopes which only slightly exceeds the internal angle of friction (i.e., 0.7, represented by white color in Fig. 6).

https://doi.org/10.5194/egusphere-2025-2088
Preprint. Discussion started: 26 May 2025

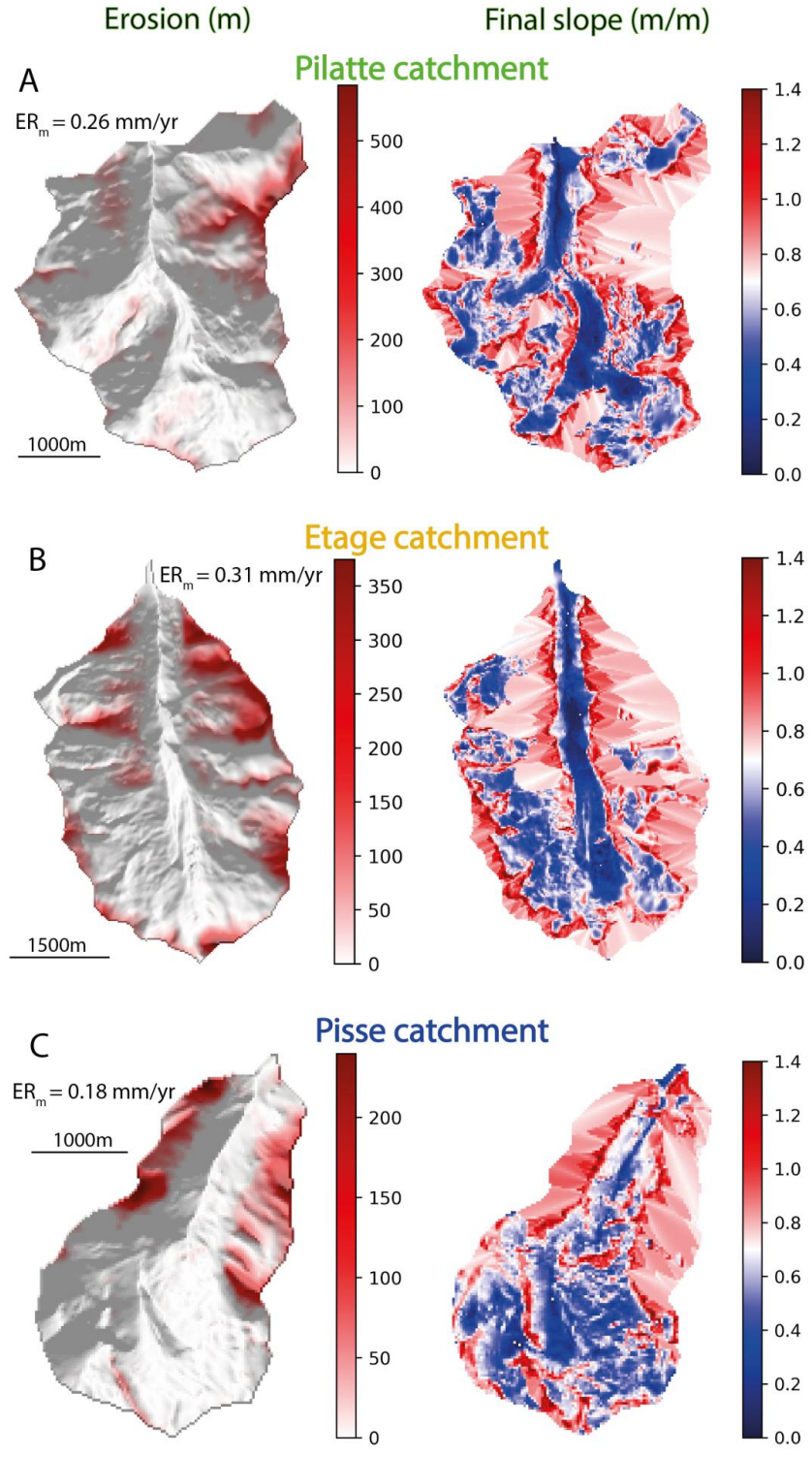

428

https://doi.org/10.5194/egusphere-2025-2088
Preprint. Discussion started: 26 May 2025

Figure 6: Simulation results of cumulative landslide erosion and final slope distribution for the studied different catchments (A - Pilatte, B - Etages, C - Pisse). Left panels display landslide erosion patterns with cumulative landslide erosion (red color) over 100-kyr simulation duration on the modern hillshade DEM. Right panels show the final slope distributions where the landslide activity results in more homogenous slope patterns around the input internal angle of friction (0.7 m/m, white colors).

4.2 Spatial distribution of landslides

For each catchment, we investigate the simulated evolution of both the hypsometric and topographic slope distributions (i.e. 2D histograms of catchment slope and elevation, Fig. 7A,D,E). As expected from the modern slope distribution (Fig. 1C), the initial catchment topographies (i.e., at 0 kyr) show a similar modal slope around 0.6 m/m. This modal slope is reached at different elevations for the different catchments: 2800, 2600 and 2600 m a.s.l. for the glacial, intermediate glacial-fluvial and fluvial catchment, respectively (Fig. 7A,D,G).

The initial model topographies of the Pilatte (glacial) and Etage (intermediate glacial-fluvial) catchments show a bimodal distribution of the elevations for steep slopes (Fig. 7A,D et 8) (Fig. S2).

The steepest slopes of the glacial catchment range between 2 and 4.5 m/m (i.e between ~63 and 77°) and are mostly restricted to the highest elevations (3000- 4000 m) (Fig. 7A). A second peak of steep slopes, with lower magnitudes (1.5 – 2.5 m/m i.e ~56° - 68°), is found around 2400 m. The intermediate glacial-fluvial catchment also shows an initial topography with two similar 'peaks' of steep slopes frequency (Fig. 8C). We observe maximum slopes around 3 m/m (~70°) between 2700 and the catchment crestline (~3500 m), and in a narrower elevation range from around 2000 to 2400 m (Fig. 7D). On the contrary, the fluvial catchment differs from the other catchments due to the relative homogeneous distribution of slopes with elevation (Fig. 7G; Fig.S3). Throughout the simulations, catchment slopes exceeding the friction angle at 0.7 m/m are affected by landslides, especially in the glacial catchment where significant changes can be noticed already after only 10 kyr simulation (Fig. 7B,E). Overall, after 100 kyr simulation, landslide activity has erased most of the steep slopes (almost three time less steep slopes, for high elevations, at the end of the simulation, Fig. 8C) , i.e. above ~1.5 m/m, reducing significantly in turn the bimodal distribution of elevation for the steep slopes (Figs. 7C,F & 8C). The maximum catchment elevation has decreased for the glacial and intermediate glacial-fluvial catchments, while it remains approximately constant for the fluvial catchment after 100 kyr of simulation.

During the simulations, we also observe a progressive increase in slope frequency slightly below 1 m/m (i.e, 45°), concentrated around 2600 – 3200 m, 2400 – 3000 m and 1900 – 2600 m for the glacial, intermediate glacial-fluvial and fluvial catchments, respectively (Figs. 7C,F,I & 8B). This new slope distribution evidences the shift from the initial steep slopes to final intermediate slopes that are closer to the input internal friction.

https://doi.org/10.5194/egusphere-2025-2088
Preprint. Discussion started: 26 May 2025

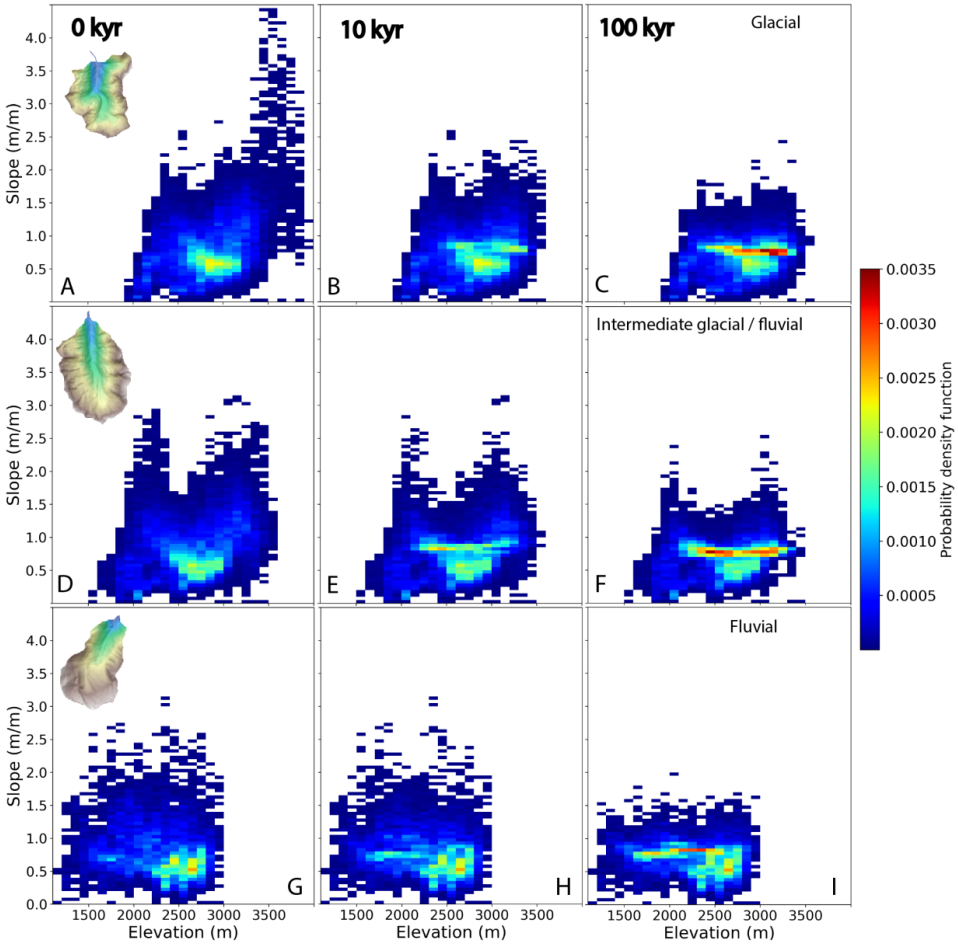

Figure 7: 2D histograms of the catchment slope distributions (color scale) with elevation. The temporal evolution of catchments slopes and elevations during simulations is monitored at three different time steps: 0, 10, an, 100 kyr (left, middle and right, respectively). Each row shows model results for a particular catchment: Pilatte (glaciated, A-B-C), Etages (intermediate glacial-fluvial, D-E-F), and Pisse (fluvial, G-H-I) . For all three catchments, steep slopes are erased and catchment slopes tend toward more homogeneous slopes around the input internal angle of friction (0.7 m/m, i.e. 35°).

https://doi.org/10.5194/egusphere-2025-2088
Preprint. Discussion started: 26 May 2025

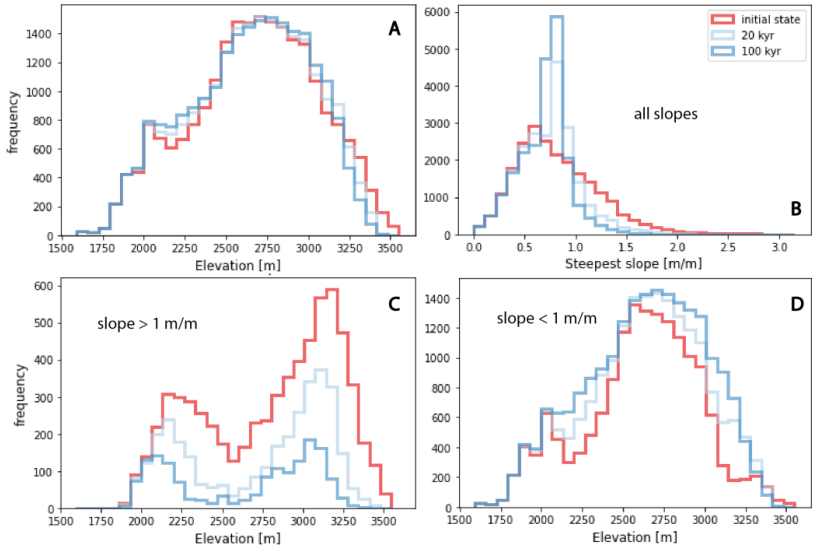

Figure 8: For the Etages catchment (intermediate glacial-fluvial), temporal evolution of (A) elevation distribution, (B) slope distribution, C-D) Elevation distribution with slope threshold values (above or below 1m/m). The colors illustrate the initial topography (red), an intermediate stage (20 kyr – light blue line) and the final topography (100 kyr – dark blue).

4.3 Temporal distribution of landslides

We now investigate the relationship between topographic changes and landslide activity (Fig. 9). Here, we identify each landslide by its time of occurrence and its triggering location, corresponding to its lowest elevation (Fig. 9). First, our results highlight the bimodal elevation distribution of the simulated landslides, roughly above 2800 m and below 2400 m, which appears persistent with time for the glacial and intermediate glacial-fluvial catchments (Fig. 9A,B). These two catchments also show an intense landslide activity for the first 20 kyr of simulation, with an apparent progressive decay with time. Large landslides occur throughout the 100 kyr of simulation time, illustrating the stochastic nature of landslide occurrence in HyLands simulations. These observations are supported by the cumulative distribution of landslides volume through simulation time (Fig. 10A-C). For the glacial and intermediate glacial-fluvial catchments, more than half of the total landslide volume is predicted before 20 kyr. However, the cumulative number of landslides increases with time for these catchments. This discrepancy between the total landslide volume and the number of landslides may illustrate the preferential occurrence of large landslides within the first 20 kyr. This interpretation is supported by the change in the probability density function of the landslide volumes after 20 kyr simulation time (Fig S5). For these two (intermediate) glacial catchments, the difference in the exponent of the power-law scaling indicates the higher frequency of large landslides within the 20 kyr of simulation time (Fig 7G-H). We do not observe this pattern for the fluvial catchment (Fig S4 C, F), although the largest landslides are still predicted during the first 20 kyr of simulation time.

https://doi.org/10.5194/egusphere-2025-2088
Preprint. Discussion started: 26 May 2025

Another interesting result is the inverse relationship between the predicted landslide volume and the number of landslides at different catchment elevations: at low elevations (<2700 m), landslides are less frequent but large landslides are overrepresented; whereas at high elevations (>2700 m), landslides are more frequent but large landslides are underrepresented. This assessment is particularly true for the Pilatte (glacial) and Etages (intermediate glacial-fluvial) catchments (Fig. 10A-B). For instance, the Pilatte catchment (Fig. 10A) displays twice more landslide occurrences at high elevations (>2700 m), with only a slightly larger eroded volume above than below 2700 m elevation.

Observations are significantly different for the fluvial catchment as the landslides are rather homogeneously distributed in the catchment (Fig. 9C). However, the high occurrences of landslides in the first 20 kyr are still noticeable (Fig. 10C) and large landslides tend to occur preferentially at low elevation (<2200 m).

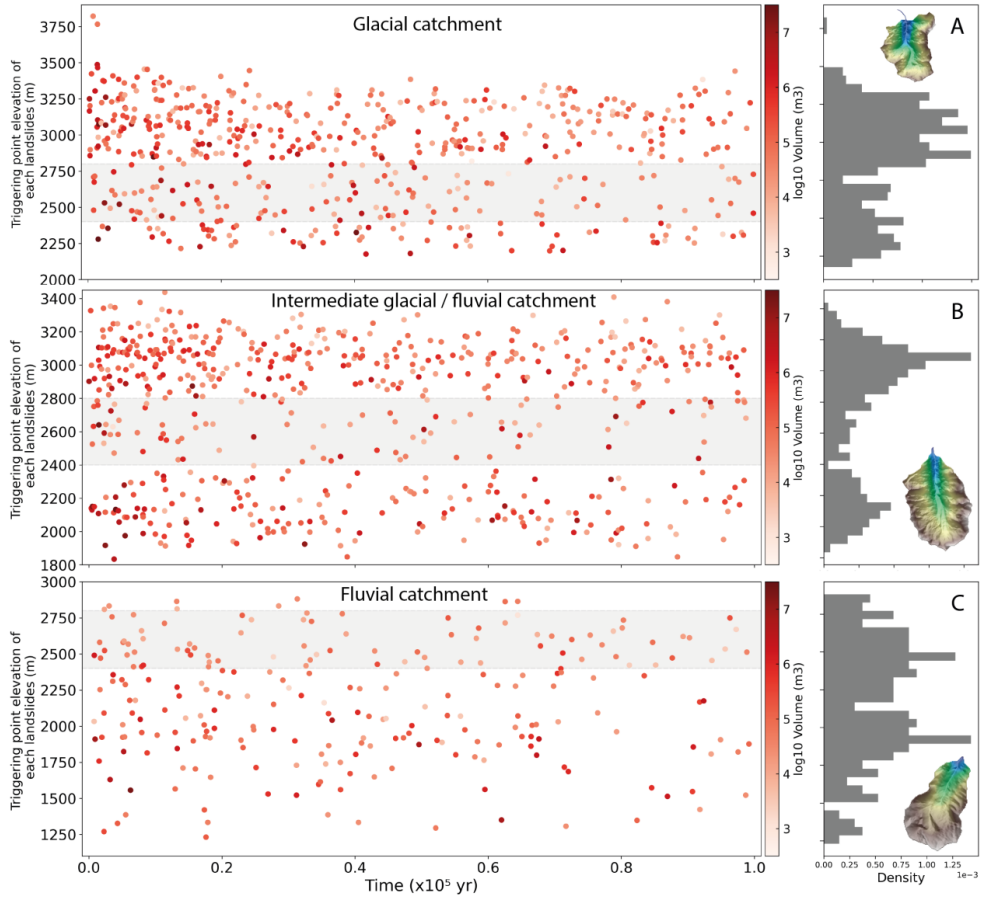

Figure 9: Triggering point elevation of each predicted landslide over the total simulation time (100 kyr) and their associated volume (red gradient colors). The landslide distributions with elevation (right panels for distributions) appear bimodal for the glacial and intermediate catchments (A - B) with two main elevation ranges around 2100 and 3000 m and no clear altitudinal distribution of predicted landslides for the fluvial catchment (C).

https://doi.org/10.5194/egusphere-2025-2088
Preprint. Discussion started: 26 May 2025

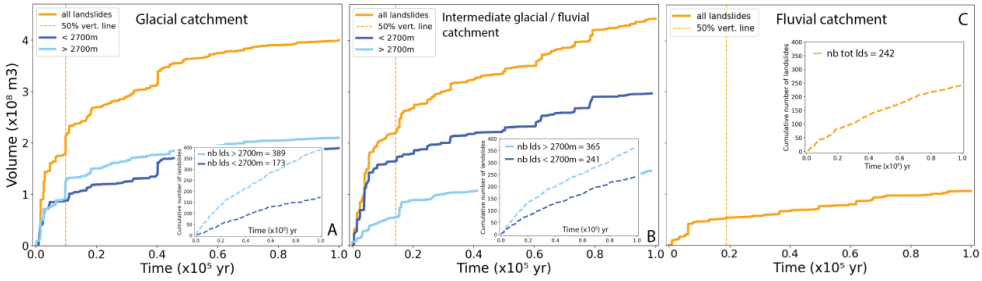

Figure 10: Cumulative distribution of the predicted landslide volumes over the total simulation time (100 kyr) for the glacial (Pilatte - A), intermediate glacial/fluvial (Etages - B) and fluvial (Pisse – C) catchments. The orange lines are the total cumulative landslide volumes, while the blue lines display the predicted cumulative volumes for landslides located above (light blue) and below (dark blue) an elevation threshold of 2700 m. The yellow vertical dashed lines indicate the simulation time when 50% of the total landslide volume is reached. Insets show the cumulative number of landslides generated during the simulation time for the two defined elevation classes.

4.4 Temporal evolution of landslide erosion rate

The term 'erosion rate' describes here only the predicted erosion induced by landslides and averaged over the catchment area. For each studied catchment, we compute the evolution of the catchment-averaged erosion rates using a 2-kyr time window, providing different statistics: mean, median, 25th and 75th percentiles of catchment-averaged erosion rates (Fig. 11). This temporal window emphasizes the general long-term trend of the predicted erosion rate by smoothing its high-frequency variations related to the stochasticity of landslide occurrence (Fig. S5). For all three catchments, the catchment-averaged erosion rates vary roughly between 10^{-5} and 10^{-1} mm/yr when at least one landslide is triggered during the time window. The predicted mean erosion rate is always significantly higher than the median erosion rate (almost 10 times at the beginning of the simulation and around 100 times after 100 kyr of simulation time), but the progressive decreasing trend is observed for both two statistical measures. In addition, the 25th percentile rapidly becomes null, highlighting that the catchment-averaged erosion rate is driven by large but infrequent landslides.

The Pilatte (glacial) catchment (Fig. 11A) shows a ~~particular~~ high mean erosion rate, above 1 mm/yr, with a rapidly decreasing trend during the first 10 kyr. Then, the mean erosion rate decreases more slowly until 60 kyr and ~~gets~~ roughly constant at 0.1-0.2 mm/yr over the last 40 kyr of simulation. A similar trend is observed for the Etages (intermediate glacial-fluvial catchment, Fig. 11B), but the initial erosion rate is ~1 mm/yr and apparently lower than for the Pilatte (glacial) catchment. ~~On the contrary,~~ the Pisse (fluvial) catchment (Fig. 11C) shows a progressive decrease in the mean erosion rate, from ~0.6 to 0.06 mm/yr after 60 kyr of simulation, with no observed peak in erosion rate at the beginning of the simulation. The median value for the fluvial catchment reaches rapidly zero within the first 20 kyr of simulation, illustrating the lower frequency of landslide occurrence compared to the glacial and intermediate glacial-fluvial catchments. Overall and for all studied catchments, predicted landslide

https://doi.org/10.5194/egusphere-2025-2088
Preprint. Discussion started: 26 May 2025

erosion rates decrease by about an order of magnitude over 100 kyr, illustrating the progressive erasing of steep slopes associated to glacial morphological features.

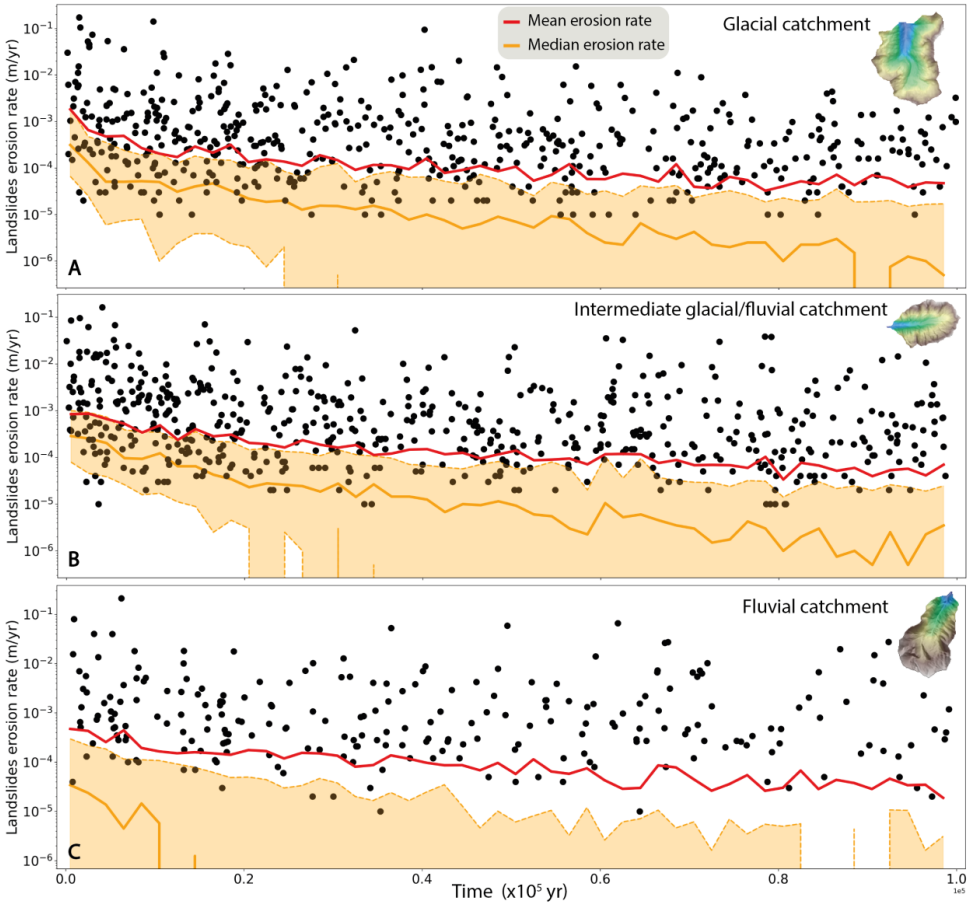

Figure 11: Temporal evolution of ~~the landslide (catchment-averaged)~~ erosion rate for the three studied catchments: A) Pilatte (glacial), B) Etages (intermediate glacial-fluvial). And C) Pisse (fluvial). Black dots illustrate the non-zero landslide erosion rates for each time step of one individual simulation, while red and orange lines depict respectively the mean and median (with 25th and 75th percentiles as dashed orange lines) erosion rates compiled from 20 individual simulations (with a smoothing temporal window of 2 kyr). For all catchments, the simulated landslide erosion rates decrease over time, especially during the first 20 kyr of simulation time, with different temporal trends depending on the catchment.

5. Discussion

5.1 Model limitations

Our landscape evolution model using HyLands has been designed to explore the hypothesis that landsliding ~~represent~~ a dominant geomorphological agent during postglacial periods. Our numerical simulations succeed in reproducing a pulse of landslides activity during the postglacial period and its

https://doi.org/10.5194/egusphere-2025-2088
Preprint. Discussion started: 26 May 2025

complex (non-homogeneous) impact on catchment hypsometry and slopes. However, this reduced-complexity model represents a simplified version of real hillslope dynamics, with limitations regarding its ability to predict in details all the richness of natural landforms, especially under the constraint of long simulation time (Tucker & Hancock, 2010). Therefore, we made several modeling choices (see Sections 3.2 and 3.3) to minimize potential feedback loops and interaction between erosion processes, which may have impacted our results as discussed below.

5.1.1 Missing processes: uplift, fluvial erosion and transport

As mentioned earlier, the model does not account for the impact of uplift, which can be considered as a limitation. Given the present-day uplift rate in the western European Alps, around 1 mm/yr (Nocquet et al., 2016; Sternai et al., 2019), the total uplift over the simulation period (100 kyr) would be around 100 m. This theoretical uplift value is of the same order of magnitude than the average decrease in elevation caused by landslide erosion in the Etages (intermediate glacial-fluvial) and Pisse (fluvial) catchments (Figs. 6-7). In the Pilatte (glacial) catchment, the mean erosion is around 26 m, with maximum cumulated erosion of ~500 m. Therefore, integrating rock uplift in the model, from either geodynamics, tectonic activity or glacial isostatic rebound (Sternai et al., 2019), could counterbalance the overall decrease in catchment elevation observed in our results. Indeed, post-glacial rebound can occur at km scale, promoting local rock uplift and potentially considered to be a significant factor in triggering landslides in some regions (~~É.~~ Cossart, 2013). In addition, rock uplift has also been proposed as modulating the post-glacial geomorphic response and landscape transition from glacial to fluvial states (Prasicek et al., 2015), ~~rock uplift~~ allowing faster relief turnover times. In addition to uplift, tectonic activity could be associated with seismicity, another well-known triggering factor for landslides (Keefer, 1984; McColl, 2012). However, our approach stays appropriate to assess the hillslope stability over 100 kyr, which is largely dependent on alpine topography, inherited from glacial-interglacial cycles, and mechanical strength. The impact of local earthquakes would mostly result in changing the timing of landslide activity, not the total volume of landslides.

The catchment-averaged erosion rate of 1 mm/yr, derived from published cosmogenic nuclide data (Delunel et al., 2010) and used for the return time calibration, is integrating a large fluvial network with multiple erosion processes (fluvial, hillslope, landslide) at the scale of the Ecrins massif. Considering effective sediment connectivity in the catchment and only landsliding to derive our catchment erosion rate, 1 mm/yr is likely to be an end member minimum value for our simulations. Therefore, we ran a supplementary simulation with a lower cohesion value (20 kPa) while keeping the same return time (150 kyr), leading overall to a higher erosion rate (about 2-3 mm/yr, Fig. 5). The simulation results show a globally higher frequency of landslides, but with similar patterns in landslide occurrence, topographic changes and temporal trend in erosion rate (Fig.S6).

https://doi.org/10.5194/egusphere-2025-2088
Preprint. Discussion started: 26 May 2025

Finally, we did not include fluvial erosion and sediment export in our simulations. Ignoring sediment transport over a long timescale (100 kyr), integrating multiple glacial-interglacial periods, is a strong model limitation for alpine erosion dynamics (Schlunegger & Hinderer, 2003). Indeed, sediment transfer dynamics over the Quaternary period is associated with glacial dynamics (Antoniazza & Lane, 2021), coupling between hillslopes and channels (Hovius et al., 2000), fluvial incision (Leith et al., 2018; Valla et al., 2010) and potential transient sediment storage (Buechi et al., 2018). Rivers are also considered as the main agent of sediment transport during interglacial period (M. N. Koppes & Montgomery, 2009; Pitlick et al., 2021). Fluvial incision also leads to a lowering of the base level, which in turn creates more steep slopes at the hillslope foot. These changes participate to renew the landslide potential of these transient landforms. However, in this study we modeled a single interglacial period and provide a focus solely on hillslopes dynamics (i.e. no fluvial dynamics); both arguments result in a lower influence of the sediment dynamics for our results.

5.1.2 Model parametrization

Our modeling strategy and parameterization have inherent limitations, such as our initial input DEM (modern alpine topography) with a low resolution (25 m). Such resolution allows long simulation periods in a reasonable simulation time with the capability to still capture first-order erosion processes and topographic changes (Campforts et al., 2022). However, this relatively low resolution may hinder potential small-scale topographic roughness that could influence both landslide occurrence and magnitude. In addition, we ran our model simulations over 100 kyr, which is longer than any interglacial period during the Quaternary.

Another strong assumption is to ignore sediment deposition on the resulting simulated topography. Landslides are among th most efficient processes for producing sediments (Keefer, 1984) in mountainous areas, which can then be available for transport from hillslopes to the drainage network. The sediment connectivity (Cavalli et al., 2019), especially for bedload sediment, from hillslopes to channels is a key indicator to quantify sediment yields and morphological changes along the source-to-sink profile (Comiti et al., 2019; Hooke, 2003; Lane et al., 2017; Micheletti et al., 2015). Thus, we explore the potential feedbacks of sediment deposition on landslide activity by testing the Hylands model with a null fine fraction parameter (Ff = 0), i.e. with a complete storage of landslide-produced sediment in the catchment. Coarse sediments are spread over the hillslopes, i.e. downstream of the landslide source, following a non-linear and non-local deposition law (Carretier et al., 2016). This deposition term depends on the transport distance which is driven by the critical slope, settled here equal to the tangent of the angle of internal friction (φ) (Campforts et al., 2022; Carretier et al., 2016).This new setup is the opposite of our main analysis (Ff =1, Section 3.2), where we assumed a perfect sediment connectivity within the catchment, leading to instantaneous sediment export. Simulated sediment storage in the catchment (Ff = 0) causes a slight increase in landslide occurrence, especially at low elevations (<2700 m). We interpret this increase as a remobilization of the sediment deposits, which

https://doi.org/10.5194/egusphere-2025-2088
Preprint. Discussion started: 26 May 2025

results in new landslide locations compared to previous simulations. The simulated deposition patterns are indeed mainly located in the valley bottom (Figs. S7-8). When the slopes of the deposits become greater than the internal angle of friction (0.7m/m, i.e. 35°), landslides can then occur. These landslides ~~trigger~~ in the sedimentary cover may also explain the slight ~~landslides increase in the shouldering~~ elevation zone (2400 – 2800 m, Figs. S7-8). However, the spatio-temporal landslide activity remains roughly similar to our previous simulations. Note that we have not computed the denudation rate without exported fine sediment because it would not be possible to compare it with measured value.

Finally, our model parameterization assumes spatially uniform model parameters both within and between the three catchments. We used a single set of calibrated cohesion and internal angle of friction values (Figs. 3-4), without differentiation based on lithology, vegetation cover, elevation or glacial cover. This assumption may limit the model capacity in capturing the complex terrain roughness of ~~alpine modern~~ topographies, which may be a factor in increasing rock resistance to sliding in natural environments. For example, in our catchment, the effect of the tree cover at low elevations may not be apprehended by the model. Thus, the expected reduction in landslide occurrence due to root reinforcement or changes in soil moisture (Muñoz et al., 2016) is not simulated. In addition, the role of high-elevation permafrost, its spatial variability and temporal evolution, on landslide activity (Magnin et al., 2017), is not captured by our simulations.

5.2 ~~The~~ spatio-temporal landslide activity over the Quaternary period

The glacial inheritance of the alpine landforms, with glacial cirques, U-shaped and hanging valleys (Fig. 3), is still a current field of investigation in terms of their formation through multiple glacial cycles of the Quaternary (Seguinot & Delaney, 2021) and their persistence during post-glacial periods (e.g. Herman & Braun, 2008; Prasicek et al., 2015). The relative contribution of glacial and fluvial erosion to Quaternary relief evolution is still debated because of the difficulties to quantify erosion over glacial-interglacial timescales (Fox et al., 2015; Shuster et al., 2005; Sternai et al., 2013; Valla et al., 2011). Moreover, some studies (M. N. Koppes & Montgomery, 2009; Leith et al., 2014, 2018; Montgomery & Korup, 2011) have argued that Late-Pleistocene glaciations had only a limited impact on Alpine topography, recent alpine relief evolution being then mainly driven by fluvial and hillslope processes during interglacial. In this context, our numerical results bring some insights into the role of these hillslope processes in the transition from glacial to fluvial morphologies.

5.2.1 Spatial landslide distribution and glacial imprint

The present-day catchment morphologies (Fig. 2) leave no doubt about the significant role of ~~the~~ glacial processes in shaping the investigated landscapes in the Ecrins massif (Fig. 1). However, our initial hypothesis about the capacity of landslides to erase this glacial topographic inheritance over the last post-glacial period is only partly validated by the simulation results.

https://doi.org/10.5194/egusphere-2025-2088
Preprint. Discussion started: 26 May 2025

First, the spatial landslide activity pattern (Fig. 9) reveals that the glacial morphologies are more subject to mass wasting processes. The steep slopes generated by glacial erosion along the U-shaped valley walls and at high elevation (crestlines and nunataks) produce a bimodal distribution of landslides with elevation, while the shouldering (Fig. 3), i.e., the gentler slope interval at mid-slope, ~~induces a weak landslides~~ activity. Therefore, our simulation results suggest that the transition from U-shaped to V-shaped valleys, as evidenced by the glacial (Pilatte) and fluvial (Pisse) catchments (Fig. 3) is highlighting the reshaping of the inherited glacial landscape through hillslope processes. However, the bimodal distribution of landslides with elevation is still noticeable after 100 kyr of simulation time (i.e., roughly ten times longer than the deglaciation period for the area). Moreover, the number of landslides and their spatial clustering is still significant for the glacial and intermediate glacial-fluvial catchments compared to the landslide pattern in the fluvial catchment (Pisse), which shows a more uniform distribution of landslides on hillslopes (Fig. 9). Thus, if the landslide activity and its spatial distribution can be considered as indicators of the hillslopes transition, our modeling results suggest that the glacial and intermediate glacial-fluvial catchments have not yet completed their post-glacial transition after 100 kyr simulation.

Second, the landslide volume distributions also illustrate a specific dynamics of mass wasting events in formerly glaciated catchments. For the upper catchments (glacial and intermediate glacial-fluvial), our modeling results suggest that landslides are more frequent at higher elevations, near the crestlines, than at lower elevation near the valley bottoms (Fig. 10). This is consistent with the recent deglaciation of the upper catchments. Indeed, nunataks and crestlines in this interior part of the massif may still benefit from the stabilizing role of permafrost. Thus, the higher elevations of the catchment (i.e., above the trimline) still display steep and sharp slopes. Under a warming climate and the degradation of permafrost, these high-elevation and steep hillslopes will potentially be more and more prone to periglacial erosion processes (as ~~it~~ is already the case for the intermediate glacial-fluvial catchment). In parallel, our simulations predict large landslides at the lower elevations (Figs. 9 & 10). These results are consistent with the effect of debuttressing (i.e., stress variations resulting from glacial unloading) along the U-shaped valley wall following glacial recession (e.g. E. Cossart et al., 2008). This is also supported by the temporal clustering of the large landslides in the first 20 kyr. Yet, the occurrence of large landslides, due to their stochastic nature, remains occasional afterwards, which is consistent with other studies (Ivy-Ochs et al., 2017; Schwartz et al., 2017; Zerathe et al., 2014).

Therefore, the persistence of landslide activity in the glacial and intermediate catchments, even after long simulation times, highlights that hillslope processes such as landslides, in response to glacial topographic inheritance, may not be the only factor explaining the fluvial morphology observed in our downstream catchment (Pisse).

https://doi.org/10.5194/egusphere-2025-2088
Preprint. Discussion started: 26 May 2025

5.2.2 Temporal landslide activity and transient topography

Here, we discuss our initial hypothesis, that all the studied catchments had the same glacial topographic imprint, and show that the three catchments have a distinct erosion dynamics explained by diachronous landslide activity following different glacial retreat times (Fig. 1). Following the previous spatial analysis (5.2.1), the observed temporal decrease in landslide occurrence and in predicted erosion rates over the first ~20 kyr (Fig. 11) reflects a decline in the proportion of unstable slopes during the post-glacial period. The faster erosion modeled for the glacial and intermediate glacial-fluvial catchments, compared to the fluvial catchment, highlights the role of landsliding as a main geomorphological agent during the transition from glacial to inter-glacial conditions. This initial and gradual pulse of erosion, which differs between the studied catchments, reflects the distinct topographic states with respect to landslide susceptibility. The glacial catchment (Pilatte) has not experienced intense periglacial processes, such as landslides, for a sufficiently long period, resulting in this high erosion rate following debutressing of unstable glacial hillslopes (E. Cossart et al., 2008). The slowing down of erosion rates in the two upper catchments (glacial and intermediate glacial-fluvial) is also illustrating this long-term transitional stage, in which hillslope processes may continue to control sediment production, but at a ~~smaller~~ pace. With few landslides occurring at the end of our simulations, and ~~associated to~~ a low erosion rate, the Pisse (fluvial) catchment could be considered at the end of its transient phase and close to "post-glacial topographic steady-state" dominated by hillslope processes (i.e no to few slope destabilizations). The modelled pulse of erosion for the postglacial phase implies that the Late Pleistocene period, marked by the transition from glacial to hillslope processes, has reactivated alpine landforms by reshaping new steep and unstable hillslopes along the U-shaped ~~valleys~~ or in the cirque areas. With its particular morphologies (Fig. 2), the glacial inheritance sustains the landslide erosion potential and may become an indicator of the glacial impact on alpine topographies. However, our model results also show that simulated landsliding over 100 kyr (duration exceeding the typical interglacial period) is not sufficient for the full transition from a glacial to a fluvial steady-state topography. Indeed, the simulated landslide activity - the bimodal landslide distribution (Fig. 9) - and the associated erosion rate are still significant at the end of our 100-kyr simulations, meaning that the hillslope system alone requires longer timescales than the typical Milankovitch cycle to reach a steady-state topography (i.e. a topography without hillslope instabilities). A longer simulation of 1 million years shows that a plateau is reached in the first 100kyr but that the erosion rate decreases gradually until 400 kyr (Fig. S9). At this time, the probability of failure is so small (probably because of no slope above the internal angle of friction), that the landslide-derived erosion rate is close to zero.

First, this observation can be compared to fluvial processes, which also have long timescales for reaching steady-state topographic conditions (Whipple, 2001). Since hillslope processes are also largely contributing to sediment production in alpine settings, the topographic response time to landsliding may play a role in the sediment cascade transfer which in turn would influence fluvial dynamics and erosion

https://doi.org/10.5194/egusphere-2025-2088
Preprint. Discussion started: 26 May 2025

rates. Second, this relatively long activity of the hillslope system during the interglacial period – calibrated from cosmogenic-nuclide derived erosion rates (section 3.3.3) - is also consistent with the absence of uplift and fluvial incision in our modeling approach. Including these model components in our simulations may decrease the duration of post-glacial landsliding activity for the studied catchments, uplift promoting faster response of the hillslope-fluvial system as observed for natural settings (Prasicek et al., 2015).

Given the long persistence of landsliding from our simulations (>100 kyr), the observed differences in landslide activity between the glacial/intermediate and fluvial catchments cannot be fully explained by the time lag in glacier retreat and the duration of the interglacial period (~10 kyr, Fig. 1). We thus propose that the glacial imprint may have been less intense in the fluvial (Pisse) catchment than in the glacial and intermediate glacial-fluvial catchments (Pilatte and Etages). This confirms the non-uniform impact of glacial processes on mountainous landforms (Herman et al., 2011; Sternai et al., 2013; van der Beek & Bourbon, 2008), resulting from different ice extent/thickness and erosion efficiency over glacial cycles (Pedersen & Egholm, 2013; Seguinot & Delaney, 2021).

5.3 Landsliding and topographic mountain evolution

5.3.1 The glacial/ interglacial transition: a hot moment for alpine erosion

Glacial erosion also does not appear to be ~~spatially-uniform~~ throughout the glacial period (Seguinot & Delaney, 2021), and field studies have shown increased glacial erosion during the deglaciation period (M. N. Koppes & Montgomery, 2009). Therefore, hot moments of glacial dynamics occur at the end of the glacial period. Following this period, our model results suggest an additional pulse of rapid erosion, associated to landsliding, at the onset of the interglacial period. Therefore, the glacial-interglacial transition seems to concentrate the most rapid rates of erosion and in turn, may ~~participate~~ strongly to landscape changes and topographic relief evolution in alpine settings.

However, our simulations were carried out on the current topography, which is already the results of 2 million years of successive glacial-interglacial cycles. Thus, the "hot-moment" of erosion that we observe in the post-glacial period occurs in U-shaped valleys that are already well marked. As landslide potential is maintained by steep slopes, this ~~shape of mature glacial valley~~ may increase ~~landslides~~ activity compared with early Quaternary activity and increase in the same time the key role of hillslopes processes in shaping long-term mountain topography (Burbank et al., 1996; Korup et al., 2007; Larsen & Montgomery, 2012).

5.3.2 Toward a "landslide buzzsaw" ?

The final landslide patterns from our simulations show interesting similarity with the morphological changes associated with the glacial buzzsaw (Fig. 6). Previous studies have highlighted the impact of glacial erosion on ~~the~~ mountain elevations and ~~reliefs,~~ referred as the 'glacial buzzsaw' (Egholm et al., 2009; Herman et al., 2013, 2021; Mitchell & Montgomery, 2006; Thomson et al., 2010; Tomkin &

https://doi.org/10.5194/egusphere-2025-2088
Preprint. Discussion started: 26 May 2025

Braun, 2002). This theoretical concept, based on the observed correlation between the position of the Equilibrium Line Altitude (ELA) and the mean and maximum height of mountains (Egholm et al., 2009), suggests that glaciers may have a strong control on mountain relief. In fact, by shaping cirques, glaciers create steep slopes at high elevations (Brozović et al., 1997), increasing erosion above the ELA. Although the ''glacial buzzsaw'' might be more complex in specific mountain ranges (Banerjee & Wani, 2018; Scherler, 2014), a concentration of surface area is usually observed around the ELA elevation (Egholm et al., 2009, 2017; Liebl et al., 2021; Pedersen et al., 2010; Prasicek et al., 2020; Steer et al., 2012).

For the three studied catchments, most of the landslide scars occur close to the catchment boundaries, i.e. along steep rock walls or ~~on sharp ridges of the catchments~~. In addition, we ~~observed~~ a decrease in the maximum catchment elevation and a concentration of hillslopes (around the angle of friction) at specific elevations (Fig. 7). Thus, our simulations highlight that the topographic slopes above the ELA seem strongly affected by landslide activity, appearing as a potential 'landslides buzzsaw' during interglacial period. This concept may not be sustainable over long time periods since landslide activity will limit the occurrence of steep hillslopes. However, over Quaternary glacial cycles, successive glaciations and associated glacial/paraglacial erosion may sustain steep hillslopes at high elevations, further promoting the "landslide buzzsaw" during subsequent interglacial periods as proposed for instance for the European Alps (Delunel et al., 2020; Norton et al., 2010). This coupling between glacial and hillslope processes would be reinforced by the topographic impact of landsliding, affecting steep hillslopes at high elevations and producing larger low-relief areas at or above the ELA (Fig. 6). This landscape conditioning would favor glacier development and erosion during the next glacial period, maintaining or enhancing the potential for glacial buzzsaw (Pedersen & Egholm, 2013).

6. Conclusions

The successive glacial-interglacial transitions during the Quaternary period have promoted landscape disequilibrium between ~~the~~ inherited topography and the dominant geomorphological processes. The HyLands model was used to study how post-glacial landslides shape alpine landscapes. We focused on landslide rates, locations, and the influence of interglacial processes on long-term landscape evolution.

We modeled the topographic evolution of three distinct catchments located in the Ecrins massif (French Alps, Fig.1), that we identified as glacial, intermediate glacial-fluvial and fluvial catchments based on their morphological characteristics (Fig. 2). For these three catchments, the highest and steepest slopes are the first topographic areas impacted by landslides (Fig. 6). Topographic changes are particularly pronounced in the glacial and intermediate catchments, where we observed a bimodal distribution of landslides corresponding to the bimodal distribution of steep slopes generated by glacial erosion. In this case, the high and steep slopes are completely erased, inducing a decrease in slopes slightly greater than the internal angle of friction (Fig. 7, 8&9). This control of hillslope processes on the maximum mountain

https://doi.org/10.5194/egusphere-2025-2088
Preprint. Discussion started: 26 May 2025

elevations and the topographic reshaping at particular elevations leads us to propose similarities between the 'glacial buzzsaw' concept and postglacial ~~landslides~~ activity.

The ~~simulation~~ results also highlight a high frequency of landslides during the first 20 kyr of our simulations (Fig. 9&10), which is associated with higher erosion rates. Landslide activity and intensity, and the resulting erosion rates, at the beginning of each simulation ~~is following~~ the morphological gradient (from glacial to fluvial) observed in our three catchments (Fig.11). Therefore, glacial topographic inheritance induces an intense post-glacial landslide activity, leading in turn possibly to regular 'hot-moments' of landscape dynamics over the Quaternary.

Our study also concludes that ~~hillslopes~~ processes, such as landslides, alone cannot drive the transient shift from glacial to fluvial morphology during ~~the~~ interglacial periods. The intensity of glacial erosion and the extent of glacial advance may have been lower in downstream areas (i.e. in this study, within the fluvial catchment), which may have led to a faster transition from glacial landscape to a fluvial one.

Finally, this study provides a basic ~~but sound~~ model for understanding landslide dynamics and their impact on alpine landscape evolution. Additional components could be incorporated to enhance the model, such as fluvial processes, permafrost degradation or non-uniform rock properties to better capture the complex interactions occurring in mountain ~~environment~~. In a future work, we intend to model the interactions between hillslope processes and glacial processes over multiple glacial-interglacial cycles to better estimate their relative contributions.

Author contributions. CA conducted the model calibration and analysis with support from BC. CA, PS and PV conceived the study and developed the methodology. All the authors were involved in writing and reviewing the paper.

Competing interests. The contact author has declared that neither they nor their co-authors have any competing interests.

Acknowledgements. The authors would like to thanks helpers who make this study easier, especially Diego Cusicanqui for the lidar extraction tool (https://doi.org/10.5281/zenodo.13832516) and Xavier Robert for his help in adapting the simple-swath Python tool (https://doi.org/10.5281/zenodo.13771754). Thanks to Boris Gailleton for his advice on coding and to Dimitri Lague for his insightful comments on landslide dynamics.

Financial support. This research has been supported by the H2020 European Research Council (grant no. 803721). PGV acknowledges support from the French ANR-PIA programme (ANR-18-MPGA-0006). BC acknowledges support from the Dutch Research Council (NWO) under the grant OCENW.M.23.027.

https://doi.org/10.5194/egusphere-2025-2088
Preprint. Discussion started: 26 May 2025

References

Anderson, R. S., Molnar, P., & Kessler, M. A. (2006). Features of glacial valley profiles simply explained. *Journal of Geophysical Research: Earth Surface*, *111*(F1). https://doi.org/10.1029/2005JF000344

Antoniazza, G., & Lane, S. N. (2021). Sediment yield over glacial cycles : A conceptual model. *Progress in Physical Geography*, *45*(6), 842-865. https://doi.org/10.1177/0309133321997292

Ballantyne, C. K. (2002). Paraglacial geomorphology. *Quaternary Science Reviews*, *21*(18), Article 18. https://doi.org/10.1016/S0277-3791(02)00005-7

Banerjee, A., & Wani, B. A. (2018). Exponentially decreasing erosion rates protect the high-elevation crests of the Himalaya. *Earth and Planetary Science Letters*, *497*, 22-28. https://doi.org/10.1016/j.epsl.2018.06.001

Barféty, J. C., Pécher, A., Bambrier, A., Demeulemeester, P., Fourneaux, J. C., Poulain, P. A., Vernet, J., & Vivier, G. (1984). Notice explicative de la feuille Saint-Christophe-en-Oisans à 1/50000. *Bureau de Recherches Géologiques et Minière: Orléans*.

Barnhart, K. R., Hutton, E. W. H., Tucker, G. E., Gasparini, N. M., Istanbulluoglu, E., Hobley, D. E. J., Lyons, N. J., Mouchene, M., Nudurupati, S. S., Adams, J. M., & Bandaragoda, C. (2020). Short communication : Landlab v2.0: a software package for Earth surface dynamics. *Earth Surface Dynamics*, *8*(2), 379-397. https://doi.org/10.5194/esurf-8-379-2020

Bennett, G. l., Molnar, P., Eisenbeiss, H., & McArdell, B. w. (2012). Erosional power in the Swiss Alps : Characterization of slope failure in the Illgraben. *Earth Surface Processes and Landforms*, *37*(15), 1627-1640. https://doi.org/10.1002/esp.3263

Blondeau, S., Gunnell, Y., & Jarman, D. (2021). Rock slope failure in the Western Alps : A first comprehensive inventory and spatial analysis. *Geomorphology*, *380*, 107622. https://doi.org/10.1016/j.geomorph.2021.107622

https://doi.org/10.5194/egusphere-2025-2088
Preprint. Discussion started: 26 May 2025

869 Brardinoni, F., & Hassan, M. A. (2007). Glacially induced organization of channel-reach morphology in
870 mountain streams. *Journal of Geophysical Research: Earth Surface*, *112*(F3).
871 https://doi.org/10.1029/2006JF000741
872 Brocklehurst, S. H., & Whipple, K. X. (2006). Assessing the relative efficiency of fluvial and glacial
873 erosion through simulation of fluvial landscapes. *Geomorphology*, *75*(3), 283-299.
874 https://doi.org/10.1016/j.geomorph.2005.07.028
875 Broeckx, J., Rossi, M., Lijnen, K., Campforts, B., Poesen, J., & Vanmaercke, M. (2020). Landslide
876 mobilization rates : A global analysis and model. *Earth-Science Reviews*, *201*, 102972.
877 https://doi.org/10.1016/j.earscirev.2019.102972
878 Brown, E. T., Stallard, R. F., Larsen, M. C., Raisbeck, G. M., & Yiou, F. (1995). Denudation rates
879 determined from the accumulation of in situ-produced 10Be in the luquillo experimental
880 forest, Puerto Rico. *Earth and Planetary Science Letters*, *129*(1), 193-202.
881 https://doi.org/10.1016/0012-821X(94)00249-X
882 Brozović, N., Burbank, D. W., & Meigs, A. J. (1997). Climatic Limits on Landscape Development in the
883 Northwestern Himalaya. *Science*, *276*(5312), 571-574.
884 https://doi.org/10.1126/science.276.5312.571
885 Buechi, M. W., Graf, H. R., Haldimann, P., Lowick, S. E., & Anselmetti, F. S. (2018). Multiple
886 Quaternary erosion and infill cycles in overdeepened basins of the northern Alpine foreland.
887 *Swiss Journal of Geosciences*, *111*(1), Article 1. https://doi.org/10.1007/s00015-017-0289-9
888 Burbank, D. W., Leland, J., Fielding, E., Anderson, R. S., Brozovic, N., Reid, M. R., & Duncan, C. (1996).
889 Bedrock incision, rock uplift and threshold hillslopes in the northwestern Himalayas. *Nature*,
890 *379*(6565), 505-510. https://doi.org/10.1038/379505a0
891 Campforts, B., Shobe, C. M., Overeem, I., & Tucker, G. E. (2022). The Art of Landslides : How
892 Stochastic Mass Wasting Shapes Topography and Influences Landscape Dynamics. *Journal of*
893 *Geophysical Research: Earth Surface*, *127*(8), e2022JF006745.
894 https://doi.org/10.1029/2022JF006745

https://doi.org/10.5194/egusphere-2025-2088
Preprint. Discussion started: 26 May 2025

Campforts, B., Shobe, C. M., Steer, P., Vanmaercke, M., Lague, D., & Braun, J. (2020). HyLands 1.0 : A hybrid landscape evolution model to simulate the impact of landslides and landslide-derived sediment on landscape evolution. *Geoscientific Model Development*, *13*(9), 3863-3886. https://doi.org/10.5194/gmd-13-3863-2020

Carretier, S., Martinod, P., Reich, M., & Godderis, Y. (2016). Modelling sediment clasts transport during landscape evolution. *Earth Surface Dynamics*, *4*(1), 237-251. https://doi.org/10.5194/esurf-4-237-2016

Carriere, A., Le Bouteiller, C., Tucker, G. E., Klotz, S., & Naaim, M. (2020). Impact of vegetation on erosion : Insights from the calibration and test of a landscape evolution model in alpine badland catchments. *Earth Surface Processes and Landforms*, *45*(5), 1085-1099. https://doi.org/10.1002/esp.4741

Cathala, M., Magnin, F., Ravanel, L., Dorren, L., Zuanon, N., Berger, F., Bourrier, F., & Deline, P. (2024). Mapping release and propagation areas of permafrost-related rock slope failures in the French Alps : A new methodological approach at regional scale. *Geomorphology*, *448*, 109032. https://doi.org/10.1016/j.geomorph.2023.109032

Cavalli, M., Heckmann, T., & Marchi, L. (2019). Sediment Connectivity in Proglacial Areas. In T. Heckmann & D. Morche (Éds.), *Geomorphology of Proglacial Systems : Landform and Sediment Dynamics in Recently Deglaciated Alpine Landscapes* (p. 271-287). Springer International Publishing. https://doi.org/10.1007/978-3-319-94184-4_16

Champagnac, J.-D., Valla, P. G., & Herman, F. (2014). Late-Cenozoic relief evolution under evolving climate : A review. *Tectonophysics*, *614*, 44-65. https://doi.org/10.1016/j.tecto.2013.11.037

Claessens, L., Schoorl, J. M., & Veldkamp, A. (2007). Modelling the location of shallow landslides and their effects on landscape dynamics in large watersheds : An application for Northern New Zealand. *Geomorphology*, *87*(1), 16-27. https://doi.org/10.1016/j.geomorph.2006.06.039

https://doi.org/10.5194/egusphere-2025-2088
Preprint. Discussion started: 26 May 2025

919 Comiti, F., Mao, L., Penna, D., Dell'Agnese, A., Engel, M., Rathburn, S., & Cavalli, M. (2019). Glacier
920 melt runoff controls bedload transport in Alpine catchments. *Earth and Planetary Science*
921 *Letters*, *520*, 77-86. https://doi.org/10.1016/j.epsl.2019.05.031
922 Cossart, É. (2013). Influence of local vs. Regional settings on glaciation patterns in the French Alps.
923 *Geografia Fisica e Dinamica Quaternaria*, *36*(1), Article 1.
924 https://doi.org/10.4461/GFDQ.2013.36.3
925 Cossart, E., Braucher, R., Fort, M., Bourlès, D. L., & Carcaillet, J. (2008). Slope instability in relation to
926 glacial debuttressing in alpine areas (Upper Durance catchment, southeastern France) :
927 Evidence from field data and 10Be cosmic ray exposure ages. *Geomorphology*, *95*(1), 3-26.
928 https://doi.org/10.1016/j.geomorph.2006.12.022
929 Coutterand, S. (2010). *Étude géomophologique des flux glaciaires dans les Alpes nord-occidentales au*
930 *Pléistocène récent. Du maximum de la dernière glaciation aux premières étapes de la*
931 *déglaciation* [Phdthesis, Université de Savoie]. https://theses.hal.science/tel-00517790
932 Croissant, T., Lague, D., Steer, P., & Davy, P. (2017). Rapid post-seismic landslide evacuation boosted
933 by dynamic river width. *Nature Geoscience*, *10*(9), Article 9.
934 https://doi.org/10.1038/ngeo3005
935 Culmann, K. (avec University of Michigan). (1875). *Die graphische Statik*. Zürich, Meyer & Zeller (A.
936 Reimann). http://archive.org/details/diegraphischest01culmgoog
937 Cusicanqui, D. (2024). *cusicand/lidarhd_ign_downloader : V3.0* (Version v3.0) [Logiciel]. Zenodo.
938 https://doi.org/10.5281/zenodo.13832516
939 Dahlquist, M. P., West, A. J., & Li, G. (2018). Landslide-driven drainage divide migration. *Geology*,
940 *46*(5), Article 5. https://doi.org/10.1130/G39916.1
941 Davy, P., Croissant, T., & Lague, D. (2017). A precipiton method to calculate river hydrodynamics,
942 with applications to flood prediction, landscape evolution models, and braiding instabilities.
943 *Journal of Geophysical Research: Earth Surface*, *122*(8), 1491-1512.
944 https://doi.org/10.1002/2016JF004156

https://doi.org/10.5194/egusphere-2025-2088
Preprint. Discussion started: 26 May 2025

Delgado, F., Zerathe, S., Schwartz, S., Mathieux, B., & Benavente, C. (2022). Inventory of large landslides along the Central Western Andes (ca. 15°–20° S) : Landslide distribution patterns and insights on controlling factors. *Journal of South American Earth Sciences*, *116*, 103824. https://doi.org/10.1016/j.jsames.2022.103824

Delunel, R., Schlunegger, F., Valla, P. G., Dixon, J., Glotzbach, C., Hippe, K., Kober, F., Molliex, S., Norton, K. P., Salcher, B., Wittmann, H., Akçar, N., & Christl, M. (2020). Late-Pleistocene catchment-wide denudation patterns across the European Alps. *Earth-Science Reviews*, *211*, 103407. https://doi.org/10.1016/j.earscirev.2020.103407

Delunel, R., van der Beek, P. A., Bourlès, D. L., Carcaillet, J., & Schlunegger, F. (2014). Transient sediment supply in a high-altitude Alpine environment evidenced through a 10Be budget of the Etages catchment (French Western Alps). *Earth Surface Processes and Landforms*, *39*(7), 890-899. https://doi.org/10.1002/esp.3494

Delunel, R., van der Beek, P. A., Carcaillet, J., Bourlès, D. L., & Valla, P. G. (2010). Frost-cracking control on catchment denudation rates : Insights from in situ produced 10Be concentrations in stream sediments (Ecrins–Pelvoux massif, French Western Alps). *Earth and Planetary Science Letters*, *293*(1), 72-83. https://doi.org/10.1016/j.epsl.2010.02.020

Densmore, A. L., Ellis, M. A., & Anderson, R. S. (1998). Landsliding and the evolution of normal-fault-bounded mountains. *Journal of Geophysical Research: Solid Earth*, *103*(B7), 15203-15219. https://doi.org/10.1029/98JB00510

Dietrich, W. E., Reiss, R., Hsu, M.-L., & Montgomery, D. R. (1995). A process-based model for colluvial soil depth and shallow landsliding using digital elevation data. *Hydrological Processes*, *9*(3-4), 383-400. https://doi.org/10.1002/hyp.3360090311

Egholm, D. L., Jansen, J. D., Brædstrup, C. F., Pedersen, V. K., Andersen, J. L., Ugelvig, S. V., Larsen, N. K., & Knudsen, M. F. (2017). Formation of plateau landscapes on glaciated continental margins. *Nature Geoscience*, *10*(8), 592-597. https://doi.org/10.1038/ngeo2980

https://doi.org/10.5194/egusphere-2025-2088
Preprint. Discussion started: 26 May 2025

970 Egholm, D. L., Nielsen, S. B., Pedersen, V. K., & Lesemann, J.-E. (2009). Glacial effects limiting
971 mountain height. *Nature*, *460*(7257), 884-887. https://doi.org/10.1038/nature08263
972 Fox, M., Herman, F., Kissling, E., & Willett, S. D. (2015). Rapid exhumation in the Western Alps driven
973 by slab detachment and glacial erosion. *Geology*, *43*(5), 379-382.
974 https://doi.org/10.1130/G36411.1
975 French, H. M. (2017). *The Periglacial Environment*. John Wiley & Sons.
976 Gallach, X., Carcaillet, J., Ravanel, L., Deline, P., Ogier, C., Rossi, M., Malet, E., & Garcia-Sellés, D.
977 (2020). Climatic and structural controls on Late-glacial and Holocene rockfall occurrence in
978 high-elevated rock walls of the Mont Blanc massif (Western Alps). *Earth Surface Processes*
979 *and Landforms*, *45*(13), 3071-3091. https://doi.org/10.1002/esp.4952
980 Ganti, V., von Hagke, C., Scherler, D., Lamb, M. P., Fischer, W. W., & Avouac, J.-P. (2016). Time scale
981 bias in erosion rates of glaciated landscapes. *Science Advances*, *2*(10), Article 10.
982 https://doi.org/10.1126/sciadv.1600204
983 George, D. L., & Iverson, R. M. (2014). A depth-averaged debris-flow model that includes the effects
984 of evolving dilatancy. II. Numerical predictions and experimental tests. *Proceedings of the*
985 *Royal Society A: Mathematical, Physical and Engineering Sciences*, *470*(2170), 20130820.
986 https://doi.org/10.1098/rspa.2013.0820
987 Guzzetti, F., Malamud, B. D., Turcotte, D. L., & Reichenbach, P. (2002). Power-law correlations of
988 landslide areas in central Italy. *Earth and Planetary Science Letters*, *195*(3), 169-183.
989 https://doi.org/10.1016/S0012-821X(01)00589-1
990 Hallet, B., Hunter, L., & Bogen, J. (1996). Rates of erosion and sediment evacuation by glaciers : A
991 review of field data and their implications. *Global and Planetary Change*, *12*(1), Article 1.
992 https://doi.org/10.1016/0921-8181(95)00021-6
993 Heimsath, A. M., Furbish, D. J., & Dietrich, W. E. (2005). The illusion of diffusion : Field evidence for
994 depth-dependent sediment transport. *Geology*, *33*(12), 949-952.
995 https://doi.org/10.1130/G21868.1

https://doi.org/10.5194/egusphere-2025-2088
Preprint. Discussion started: 26 May 2025

996 Hergarten, S., & Robl, J. (2015). Modelling rapid mass movements using the shallow water equations
997 in Cartesian coordinates. *Natural Hazards and Earth System Sciences*, *15*(3), 671-685.
998 https://doi.org/10.5194/nhess-15-671-2015
999 Herman, F., Beaud, F., Champagnac, J.-D., Lemieux, J.-M., & Sternai, P. (2011). Glacial hydrology and
1000 erosion patterns : A mechanism for carving glacial valleys. *Earth and Planetary Science*
1001 *Letters*, *310*(3), 498-508. https://doi.org/10.1016/j.epsl.2011.08.022
1002 Herman, F., & Braun, J. (2008). Evolution of the glacial landscape of the Southern Alps of New
1003 Zealand : Insights from a glacial erosion model. *Journal of Geophysical Research: Earth*
1004 *Surface*, *113*(F2). https://doi.org/10.1029/2007JF000807
1005 Herman, F., & Champagnac, J.-D. (2016). Plio-Pleistocene increase of erosion rates in mountain belts
1006 in response to climate change. *Terra Nova*, *28*(1), 2-10. https://doi.org/10.1111/ter.12186
1007 Herman, F., De Doncker, F., Delaney, I., Prasicek, G., & Koppes, M. (2021). The impact of glaciers on
1008 mountain erosion. *Nature Reviews Earth & Environment*, *2*(6), 422-435.
1009 https://doi.org/10.1038/s43017-021-00165-9
1010 Herman, F., Seward, D., Valla, P. G., Carter, A., Kohn, B., Willett, S. D., & Ehlers, T. A. (2013).
1011 Worldwide acceleration of mountain erosion under a cooling climate. *Nature*, *504*(7480),
1012 423-426. https://doi.org/10.1038/nature12877
1013 Hobley, D. E. J., Adams, J. M., Nudurupati, S. S., Hutton, E. W. H., Gasparini, N. M., Istanbulluoglu, E.,
1014 & Tucker, G. E. (2017). Creative computing with Landlab : An open-source toolkit for building,
1015 coupling, and exploring two-dimensional numerical models of Earth-surface dynamics. *Earth*
1016 *Surface Dynamics*, *5*(1), 21-46. https://doi.org/10.5194/esurf-5-21-2017
1017 Hooke, J. (2003). Coarse sediment connectivity in river channel systems : A conceptual framework
1018 and methodology. *Geomorphology*, *56*(1), Article 1. https://doi.org/10.1016/S0169-
1019 555X(03)00047-3

https://doi.org/10.5194/egusphere-2025-2088
Preprint. Discussion started: 26 May 2025

Hovius, N., Stark, C. P., & Allen, P. A. (1997). Sediment flux from a mountain belt derived by landslide mapping. *Geology*, *25*(3), 231-234. https://doi.org/10.1130/0091-7613(1997)025<0231:SFFAMB>2.3.CO;2

Hovius, N., Stark, C. P., Hao-Tsu, C., & Jiun-Chuan, L. (2000). Supply and Removal of Sediment in a Landslide-Dominated Mountain Belt : Central Range, Taiwan. *The Journal of Geology*, *108*(1), 73-89. https://doi.org/10.1086/314387

Ivy-Ochs, S., Martin, S., Campedel, P., Hippe, K., Alfimov, V., Vockenhuber, C., Andreotti, E., Carugati, G., Pasqual, D., Rigo, M., & Viganò, A. (2017). Geomorphology and age of the Marocche di Dro rock avalanches (Trentino, Italy). *Quaternary Science Reviews*, *169*, 188-205. https://doi.org/10.1016/j.quascirev.2017.05.014

Jeandet, L., Steer, P., Lague, D., & Davy, P. (2019). *Coulomb Mechanics and Relief Constraints Explain Landslide Size Distribution—Jeandet—2019—Geophysical Research Letters—Wiley Online Library*. https://agupubs.onlinelibrary.wiley.com/doi/full/10.1029/2019GL082351

Keefer, D. K. (1984). Landslides caused by earthquakes. *GSA Bulletin*, *95*(4), 406-421. https://doi.org/10.1130/0016-7606(1984)95<406:LCBE>2.0.CO;2

Koppes, M., Hallet, B., Rignot, E., Mouginot, J., Wellner, J. S., & Boldt, K. (2015). Observed latitudinal variations in erosion as a function of glacier dynamics. *Nature*, *526*(7571), 100-103. https://doi.org/10.1038/nature15385

Koppes, M. N., & Montgomery, D. R. (2009). The relative efficacy of fluvial and glacial erosion over modern to orogenic timescales. *Nature Geoscience*, *2*(9), 644-647. https://doi.org/10.1038/ngeo616

Korup, O. (2006). Effects of large deep-seated landslides on hillslope morphology, western Southern Alps, New Zealand. *Journal of Geophysical Research: Earth Surface*, *111*(F1), Article F1. https://doi.org/10.1029/2004JF000242

https://doi.org/10.5194/egusphere-2025-2088
Preprint. Discussion started: 26 May 2025

Korup, O., Clague, J. J., Hermanns, R. L., Hewitt, K., Strom, A. L., & Weidinger, J. T. (2007). Giant landslides, topography, and erosion. *Earth and Planetary Science Letters*, *261*(3), 578-589. https://doi.org/10.1016/j.epsl.2007.07.025

Kuhlemann, J., Frisch, W., Székely, B., Dunkl, I., & Kázmér, M. (2002). Post-collisional sediment budget history of the Alps : Tectonic versus climatic control. *International Journal of Earth Sciences*, *91*(5), 818-837. https://doi.org/10.1007/s00531-002-0266-y

Lane, S. N., Bakker, M., Gabbud, C., Micheletti, N., & Saugy, J.-N. (2017). Sediment export, transient landscape response and catchment-scale connectivity following rapid climate warming and Alpine glacier recession. *Geomorphology*, *277*, 210-227. https://doi.org/10.1016/j.geomorph.2016.02.015

Langston, A. L., & Tucker, G. E. (2018). Developing and exploring a theory for the lateral erosion of bedrock channels for use in landscape evolution models. *Earth Surface Dynamics*, *6*(1), Article 1. https://doi.org/10.5194/esurf-6-1-2018

Larsen, I. J., & Montgomery, D. R. (2012). Landslide erosion coupled to tectonics and river incision. *Nature Geoscience*, *5*(7), 468-473. https://doi.org/10.1038/ngeo1479

Lavé, J., Guérin, C., Valla, P. G., Guillou, V., Rigaudier, T., Benedetti, L., France-Lanord, C., Gajurel, A. P., Morin, G., Dumoulin, J. P., Moreau, C., & Galy, V. (2023). Medieval demise of a Himalayan giant summit induced by mega-landslide. *Nature*, *619*(7968), 94-101. https://doi.org/10.1038/s41586-023-06040-5

Le Roy, M., Deline, P., Carcaillet, J., Schimmelpfennig, I., & Ermini, M. (2017). 10Be exposure dating of the timing of Neoglacial glacier advances in the Ecrins-Pelvoux massif, southern French Alps. *Quaternary Science Reviews*, *178*, 118-138. https://doi.org/10.1016/j.quascirev.2017.10.010

Lebrouc, V., Schwartz, S., Baillet, L., Jongmans, D., & Gamond, J. F. (2013). Modeling permafrost extension in a rock slope since the Last Glacial Maximum : Application to the large Séchilienne landslide (French Alps). *Geomorphology*, *198*, 189-200. https://doi.org/10.1016/j.geomorph.2013.06.001

https://doi.org/10.5194/egusphere-2025-2088
Preprint. Discussion started: 26 May 2025

Lehmann, B., & Robert, X. (2024). *Simple_swath, a simple Python code to extract swath profile using a shapefile* (Version 2.0.0) [Logiciel]. Zenodo. https://doi.org/10.5281/zenodo.13771754

Leith, K., Fox, M., & Moore, J. R. (2018). Signatures of Late Pleistocene fluvial incision in an Alpine landscape. *Earth and Planetary Science Letters*, *483*, 13-28. https://doi.org/10.1016/j.epsl.2017.11.050

Leith, K., Moore, J. R., Amann, F., & Loew, S. (2014). Subglacial extensional fracture development and implications for Alpine Valley evolution. *Journal of Geophysical Research: Earth Surface*, *119*(1), 62-81. https://doi.org/10.1002/2012JF002691

Liebl, M., Robl, J., Egholm, D. L., Prasicek, G., Stüwe, K., Gradwohl, G., & Hergarten, S. (2021). Topographic signatures of progressive glacial landscape transformation. *Earth Surface Processes and Landforms*, *46*(10), 1964-1980. https://doi.org/10.1002/esp.5139

Louis, H. (1952). Zur Theorie der Gletschererosion in Tälern. *E&G Quaternary Science Journal*, *2*(1), 12-24. https://doi.org/10.3285/eg.02.1.02

Magnin, F., Josnin, J.-Y., Ravanel, L., Pergaud, J., Pohl, B., & Deline, P. (2017). Modelling rock wall permafrost degradation in the Mont Blanc massif from the LIA to the end of the 21st century. *The Cryosphere*, *11*(4), 1813-1834. https://doi.org/10.5194/tc-11-1813-2017

Malamud, B. D., Turcotte, D. L., Guzzetti, F., & Reichenbach, P. (2004). Landslide inventories and their statistical properties. *Earth Surface Processes and Landforms*, *29*(6), 687-711. https://doi.org/10.1002/esp.1064

Martin, H. A., Peruzzetto, M., Viroulet, S., Mangeney, A., Lagrée, P.-Y., Popinet, S., Maury, B., Lefebvre-Lepot, A., Maday, Y., & Bouchut, F. (2023). Numerical simulations of granular dam break : Comparison between discrete element, Navier-Stokes, and thin-layer models. *Physical Review E*, *108*(5), 054902. https://doi.org/10.1103/PhysRevE.108.054902

Marx, H. E., Dentant, C., Renaud, J., Delunel, R., Tank, D. C., & Lavergne, S. (2017). Riders in the sky (islands) : Using a mega-phylogenetic approach to understand plant species distribution and

https://doi.org/10.5194/egusphere-2025-2088
Preprint. Discussion started: 26 May 2025

coexistence at the altitudinal limits of angiosperm plant life. *Journal of Biogeography*, *44*(11), 2618-2630. https://doi.org/10.1111/jbi.13073

McColl, S. T. (2012). Paraglacial rock-slope stability. *Geomorphology*, *153-154*, 1-16. https://doi.org/10.1016/j.geomorph.2012.02.015

Métivier, F., Gaudemer, Y., Tapponnier, P., & Klein, M. (1999). Mass accumulation rates in Asia during the Cenozoic. *Geophysical Journal International*, *137*(2), 280-318. https://doi.org/10.1046/j.1365-246X.1999.00802.x

Meunier, P., Hovius, N., & Haines, J. A. (2008). Topographic site effects and the location of earthquake induced landslides. *Earth and Planetary Science Letters*, *275*(3), 221-232. https://doi.org/10.1016/j.epsl.2008.07.020

Micheletti, N., Lambiel, C., & Lane, S. N. (2015). Investigating decadal-scale geomorphic dynamics in an alpine mountain setting. *Journal of Geophysical Research: Earth Surface*, *120*(10), Article 10. https://doi.org/10.1002/2015JF003656

Mitchell, S. G., & Montgomery, D. R. (2006). Influence of a glacial buzzsaw on the height and morphology of the Cascade Range in central Washington State, USA. *Quaternary Research*, *65*(1), 96-107. https://doi.org/10.1016/j.yqres.2005.08.018

Montgomery, D. R., & Korup, O. (2011). Preservation of inner gorges through repeated Alpine glaciations. *Nature Geoscience*, *4*(1), 62-67. https://doi.org/10.1038/ngeo1030

Morriss, M. C., Lehmann, B., Campforts, B., Brencher, G., Rick, B., Anderson, L. S., Handwerger, A. L., Overeem, I., & Moore, J. (2023). Alpine hillslope failure in the western US : Insights from the Chaos Canyon landslide, Rocky Mountain National Park, USA. *Earth Surface Dynamics*, *11*(6), 1251-1274. https://doi.org/10.5194/esurf-11-1251-2023

Mudd, S. M., Harel, M.-A., Hurst, M. D., Grieve, S. W. D., & Marrero, S. M. (2016). The CAIRN method : Automated, reproducible calculation of catchment-averaged denudation rates from cosmogenic nuclide concentrations. *Earth Surface Dynamics*, *4*(3), 655-674. https://doi.org/10.5194/esurf-4-655-2016

https://doi.org/10.5194/egusphere-2025-2088
Preprint. Discussion started: 26 May 2025

Müller, T., Lane, S. N., & Schaefli, B. (2022). Towards a hydrogeomorphological understanding of proglacial catchments : An assessment of groundwater storage and release in an Alpine catchment. *Hydrology and Earth System Sciences*, *26*(23), 6029-6054. https://doi.org/10.5194/hess-26-6029-2022

Muñoz, E., Ochoa, A., & Cordão-Neto, M. (2016). Probabilistic assessment of precipitation-triggered landslides : The role of vegetation. *E3S Web of Conferences*, *9*, 08001. https://doi.org/10.1051/e3sconf/20160908001

Nocquet, J.-M., Sue, C., Walpersdorf, A., Tran, T., Lenôtre, N., Vernant, P., Cushing, M., Jouanne, F., Masson, F., Baize, S., Chéry, J., & van der Beek, P. A. (2016). Present-day uplift of the western Alps. *Scientific Reports*, *6*(1), Article 1. https://doi.org/10.1038/srep28404

Norton, K. P., Abbühl, L. M., & Schlunegger, F. (2010). Glacial conditioning as an erosional driving force in the Central Alps. *Geology*, *38*(7), 655-658. https://doi.org/10.1130/G31102.1

Pedersen, V. K., & Egholm, D. L. (2013). Glaciations in response to climate variations preconditioned by evolving topography. *Nature*, *493*(7431), 206-210. https://doi.org/10.1038/nature11786

Pedersen, V. K., Egholm, D. L., & Nielsen, S. B. (2010). Alpine glacial topography and the rate of rock column uplift : A global perspective. *Geomorphology*, *122*(1), 129-139. https://doi.org/10.1016/j.geomorph.2010.06.005

Peizhen, Z., Molnar, P., & Downs, W. R. (2001). Increased sedimentation rates and grain sizes 2–4 Myr ago due to the influence of climate change on erosion rates. *Nature*, *410*(6831), 891-897. https://doi.org/10.1038/35073504

Penck, A. (1905). Glacial Features in the Surface of the Alps. *The Journal of Geology*, *13*(1), 1-19. https://doi.org/10.1086/621202

Perron, J. T. (2011). Numerical methods for nonlinear hillslope transport laws. *Journal of Geophysical Research: Earth Surface*, *116*(F2). https://doi.org/10.1029/2010JF001801

https://doi.org/10.5194/egusphere-2025-2088
Preprint. Discussion started: 26 May 2025

1145 Pitlick, J., Recking, A., Liebault, F., Misset, C., Piton, G., & Vazquez-Tarrio, D. (2021). Sediment
1146 Production in French Alpine Rivers. *Water Resources Research*, *57*(12), e2021WR030470.
1147 https://doi.org/10.1029/2021WR030470
1148 Portenga, E. W., & Bierman, P. R. (2011). Understanding earth's eroding surface with ^{10}Be. *College of*
1149 *Arts and Sciences Faculty Publications*. https://doi.org/10.1130/G111A.1
1150 Prasicek, G., Hergarten, S., Deal, E., Herman, F., & Robl, J. (2020). A glacial buzzsaw effect generated
1151 by efficient erosion of temperate glaciers in a steady state model. *Earth and Planetary*
1152 *Science Letters*, *543*, 116350. https://doi.org/10.1016/j.epsl.2020.116350
1153 Prasicek, G., Larsen, I. J., & Montgomery, D. R. (2015). Tectonic control on the persistence of glacially
1154 sculpted topography. *Nature Communications*, *6*(1), 8028.
1155 https://doi.org/10.1038/ncomms9028
1156 Ravanel, L., Magnin, F., & Deline, P. (2017). Impacts of the 2003 and 2015 summer heatwaves on
1157 permafrost-affected rock-walls in the Mont Blanc massif. *Science of The Total Environment*,
1158 *609*, 132-143. https://doi.org/10.1016/j.scitotenv.2017.07.055
1159 Roering, J. (2012). Landslides limit mountain relief. *Nature Geoscience*, *5*(7), 446-447.
1160 https://doi.org/10.1038/ngeo1511
1161 Roering, J. J., Kirchner, J. W., & Dietrich, W. E. (1999). Evidence for nonlinear, diffusive sediment
1162 transport on hillslopes and implications for landscape morphology. *Water Resources*
1163 *Research*, *35*(3), 853-870. https://doi.org/10.1029/1998WR900090
1164 Rootes, C. M., & Clark, C. D. (2020). Glacial trimlines to identify former ice margins and subglacial
1165 thermal boundaries : A review and classification scheme for trimline expression. *Earth-*
1166 *Science Reviews*, *210*, 103355. https://doi.org/10.1016/j.earscirev.2020.103355
1167 Roussel, E., Marren, P. M., Cossart, E., Toumazet, J.-P., Chenet, M., Grancher, D., & Jomelli, V. (2018).
1168 Incision and aggradation in proglacial rivers : Post-Little Ice Age long-profile adjustments of
1169 Southern Iceland outwash plains. *Land Degradation & Development*, *29*(10), 3753-3771.
1170 https://doi.org/10.1002/ldr.3127

https://doi.org/10.5194/egusphere-2025-2088
Preprint. Discussion started: 26 May 2025

Scherler, D. (2014). Climatic limits to headwall retreat in the Khumbu Himalaya, eastern Nepal. *Geology*, *42*(11), 1019-1022. https://doi.org/10.1130/G35975.1

Schlunegger, F., & Hinderer, M. (2003). Pleistocene/Holocene climate change, re-establishment of fluvial drainage network and increase in relief in the Swiss Alps. *Terra Nova*, *15*(2), 88-95. https://doi.org/10.1046/j.1365-3121.2003.00469.x

Schwartz, S., Zerathe, S., Jongmans, D., Baillet, L., Carcaillet, J., Audin, L., Dumont, T., Bourlès, D., Braucher, R., & Lebrouc, V. (2017). Cosmic ray exposure dating on the large landslide of Séchilienne (Western Alps) : A synthesis to constrain slope evolution. *Geomorphology*, *278*, 329-344. https://doi.org/10.1016/j.geomorph.2016.11.014

Seguinot, J., & Delaney, I. (2021). Last-glacial-cycle glacier erosion potential in the Alps. *Earth Surface Dynamics*, *9*(4), 923-935. https://doi.org/10.5194/esurf-9-923-2021

Shuster, D. L., Ehlers, T. A., Rusmoren, M. E., & Farley, K. A. (2005). Rapid Glacial Erosion at 1.8 Ma Revealed by 4He/3He Thermochronometry. *Science*, *310*(5754), 1668-1670. https://doi.org/10.1126/science.1118519

Solomina, O. N., Bradley, R. S., Hodgson, D. A., Ivy-Ochs, S., Jomelli, V., Mackintosh, A. N., Nesje, A., Owen, L. A., Wanner, H., Wiles, G. C., & Young, N. E. (2015). Holocene glacier fluctuations. *Quaternary Science Reviews*, *111*, 9-34. https://doi.org/10.1016/j.quascirev.2014.11.018

Stark, C. P., & Hovius, N. (2001). The characterization of landslide size distributions. *Geophysical Research Letters*, *28*(6), 1091-1094. https://doi.org/10.1029/2000GL008527

Steer, P., Huismans, R. S., Valla, P. G., Gac, S., & Herman, F. (2012). Bimodal Plio–Quaternary glacial erosion of fjords and low-relief surfaces in Scandinavia. *Nature Geoscience*, *5*(9), Article 9. https://doi.org/10.1038/ngeo1549

Sternai, P., Herman, F., Valla, P. G., & Champagnac, J.-D. (2013). Spatial and temporal variations of glacial erosion in the Rhône valley (Swiss Alps) : Insights from numerical modeling. *Earth and Planetary Science Letters*, *368*, 119-131. https://doi.org/10.1016/j.epsl.2013.02.039

https://doi.org/10.5194/egusphere-2025-2088
Preprint. Discussion started: 26 May 2025

Sternai, P., Sue, C., Husson, L., Serpelloni, E., Becker, T. W., Willett, S. D., Faccenna, C., Di Giulio, A., Spada, G., Jolivet, L., Valla, P., Petit, C., Nocquet, J.-M., Walpersdorf, A., & Castelltort, S. (2019). Present-day uplift of the European Alps : Evaluating mechanisms and models of their relative contributions. *Earth-Science Reviews*, *190*, 589-604. https://doi.org/10.1016/j.earscirev.2019.01.005

Stoffel, M., Trappmann, D. G., Coullie, M. I., Ballesteros Cánovas, J. A., & Corona, C. (2024). Rockfall from an increasingly unstable mountain slope driven by climate warming. *Nature Geoscience*, 1-6. https://doi.org/10.1038/s41561-024-01390-9

Tanyaş, H., Allstadt, K. E., & van Westen, C. J. (2018). An updated method for estimating landslide-event magnitude. *Earth Surface Processes and Landforms*, *43*(9), 1836-1847. https://doi.org/10.1002/esp.4359

Tanyaş, H., van Westen, C. J., Allstadt, K. E., & Jibson, R. W. (2019). Factors controlling landslide frequency–area distributions. *Earth Surface Processes and Landforms*, *44*(4), 900-917. https://doi.org/10.1002/esp.4543

Tebbens, S. F. (2020). *Landslide Scaling : A Review—Tebbens—2020—Earth and Space Science—Wiley Online Library*. https://agupubs.onlinelibrary.wiley.com/doi/full/10.1029/2019EA000662

Thomson, S. N., Brandon, M. T., Tomkin, J. H., Reiners, P. W., Vásquez, C., & Wilson, N. J. (2010). Glaciation as a destructive and constructive control on mountain building. *Nature*, *467*(7313), 313-317. https://doi.org/10.1038/nature09365

Tomkin, J. H., & Braun, J. (2002). The influence of alpine glaciation on the relief of tectonically active mountain belts. *American Journal of Science*, *302*(3), 169-190. https://doi.org/10.2475/ajs.302.3.169

Tucker, G. E., & Hancock, G. R. (2010). Modelling landscape evolution. *Earth Surface Processes and Landforms*, *35*(1), 28-50. https://doi.org/10.1002/esp.1952

https://doi.org/10.5194/egusphere-2025-2088
Preprint. Discussion started: 26 May 2025

Valla, P. G. (2021). A tribute to Louis (1952) : On the theory of glacial erosion in valleys. *E&G Quaternary Science Journal*, *70*(2), 209-212. https://doi.org/10.5194/egqsj-70-209-2021

Valla, P. G., Shuster, D. L., & van der Beek, P. A. (2011). Significant increase in relief of the European Alps during mid-Pleistocene glaciations. *Nature Geoscience*, *4*(10), 688-692. https://doi.org/10.1038/ngeo1242

Valla, P. G., van der Beek, P. A., & Lague, D. (2010). Fluvial incision into bedrock : Insights from morphometric analysis and numerical modeling of gorges incising glacial hanging valleys (Western Alps, France). *Journal of Geophysical Research: Earth Surface*, *115*(F2). https://doi.org/10.1029/2008JF001079

Van Den Eeckhaut, M., Poesen, J., Govers, G., Verstraeten, G., & Demoulin, A. (2007). Characteristics of the size distribution of recent and historical landslides in a populated hilly region. *Earth and Planetary Science Letters*, *256*(3), 588-603. https://doi.org/10.1016/j.epsl.2007.01.040

van der Beek, P., & Bourbon, P. (2008). A quantification of the glacial imprint on relief development in the French western Alps. *Geomorphology*, *97*(1), Article 1. https://doi.org/10.1016/j.geomorph.2007.02.038

von Blanckenburg, F. (2005). The control mechanisms of erosion and weathering at basin scale from cosmogenic nuclides in river sediment. *Earth and Planetary Science Letters*, *237*(3), 462-479. https://doi.org/10.1016/j.epsl.2005.06.030

Whipple, K. X. (2001). Fluvial Landscape Response Time : How Plausible Is Steady-State Denudation? *American Journal of Science*, *301*(4-5), 313-325. https://doi.org/10.2475/ajs.301.4-5.313

Wood, J. L., Harrison, S., & Reinhardt, L. (2015). Landslide inventories for climate impacts research in the European Alps. *Geomorphology*, *228*, 398-408. https://doi.org/10.1016/j.geomorph.2014.09.005

Zachos, J., Pagani, M., Sloan, L., Thomas, E., & Billups, K. (2001). Trends, Rhythms, and Aberrations in Global Climate 65 Ma to Present. *Science*, *292*(5517), 686-693. https://doi.org/10.1126/science.1059412

https://doi.org/10.5194/egusphere-2025-2088
Preprint. Discussion started: 26 May 2025

1247 Zech, R., Zech, M., Kubik, P. W., Kharki, K., & Zech, W. (2009). Deglaciation and landscape history
1248 around Annapurna, Nepal, based on 10Be surface exposure dating. *Quaternary Science*
1249 *Reviews*, *28*(11), 1106-1118. https://doi.org/10.1016/j.quascirev.2008.11.013
1250 Zerathe, S., Lebourg, T., Braucher, R., & Bourlès, D. (2014). Mid-Holocene cluster of large-scale
1251 landslides revealed in the Southwestern Alps by 36Cl dating. Insight on an Alpine-scale
1252 landslide activity. *Quaternary Science Reviews*, *90*, 106-127.
1253 https://doi.org/10.1016/j.quascirev.2014.02.015
1254 Zhang, T., Li, D., East, A. E., Walling, D. E., Lane, S., Overeem, I., Beylich, A. A., Koppes, M., & Lu, X.
1255 (2022). Warming-driven erosion and sediment transport in cold regions. *Nature Reviews*
1256 *Earth & Environment*, *3*(12), 832-851. https://doi.org/10.1038/s43017-022-00362-0
1257
1258